

COPY NO. 97

RM No. E7A28

~~RESTRICTED~~
NACA

RESEARCH MEMORANDUM

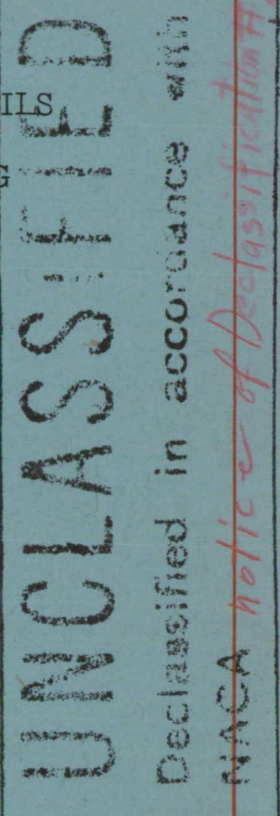
VELOCITY DISTRIBUTIONS ON ARBITRARY AIRFOILS
IN CLOSED TUNNELS BY CONFORMAL MAPPING

By H. E. Moses

Aircraft Engine Research Laboratory
Cleveland, Ohio

~~CLASSIFIED DOCUMENT~~

This document contains classified information affecting the National Defense of the United States within the meaning of the Espionage Act, USC 50:31 and 32. Its transmission or the revelation of its contents in any manner to an unauthorized person is prohibited by law. Information so classified may be imparted only to persons in the military and naval Services of the United States, appropriate civilian officers and employees of the Federal Government who have a legitimate interest therein, and to United States citizens known loyalty and discretion who of necessity must be informed thereof.



**NATIONAL ADVISORY COMMITTEE
FOR AERONAUTICS**

WASHINGTON

January 28, 1947

~~RESTRICTED~~

NATIONAL ADVISORY COMMITTEE FOR AERONAUTICS

RESEARCH MEMORANDUM

VELOCITY DISTRIBUTIONS ON ARBITRARY AIRFOILS

IN CLOSED TUNNELS BY CONFORMAL MAPPING

By H. E. Moses

SUMMARY

Conformal mapping methods are applied to the calculation of the effect of channel (two-dimensional tunnel) walls on the ideal flow past arbitrary airfoils situated anywhere within the channel. The walls of the channel need not be plane but may have any shape. The results are compared in specific cases with those obtained by two approximate methods, of which the first is a first-order treatment using image vortices and doublets and the second is a higher-order correction developed by Goldstein.

INTRODUCTION

In reference 1 a conformal mapping method was developed whereby the zero-lift velocity distribution could be found for a symmetrical airfoil symmetrically located in a plane-walled channel. The purpose of the present paper is to extend the previous investigation to the case of an arbitrary airfoil situated anywhere within an arbitrarily shaped channel (two-dimensional tunnel).

The Cartesian mapping function (CMF), introduced in reference 2 and used in the method of reference 1, is also used for the problem of the present paper. The velocity at any point on the airfoil in the channel is found in terms of the CMF and the known conformal transformation of a flat plate in a channel. The difference between this velocity and the velocity at the same point on the isolated airfoil at the same angle of attack represents the effect of the channel walls. In order to obtain the velocity distribution on the airfoil within the channel, the CMF is applied to doubly connected regions analogously to the manner in which Theodorsen's mapping function is applied in reference 3.

The method is given, illustrated numerically by examples, and compared with corresponding results by the first-order image theory

and by the second-order image theory of Goldstein (reference 4). In addition to the velocity on the airfoil, the velocity on the channel walls is obtained by the conformal mapping method.

SYMBOLS

The more important symbols used in this paper are listed as follows:

c	chord of airfoil
c_l	section lift coefficient for isolated airfoil
$c_{l\prime}$	section lift coefficient for airfoil in channel
h	distance between channel walls
t	thickness of airfoil
v	undisturbed velocity at great distance from airfoil
v_{cl}	velocity on surface of airfoil in channel
v_{c2}	velocity on channel walls
v_i	velocity on isolated airfoil
Δv	velocity correction, $v_{cl} - v_i$
α	angle of attack of airfoil
$\bar{\alpha}$	angle of attack of flat plate
α_1	effective angle of attack of airfoil with respect to curved stream
ζ	plane of straight lines
z	physical plane
p	circle plane

METHOD OF CONFORMAL MAPPING

The CMF for One Contour

In previous applications of the conformal mapping method used in the present paper (for example, references 1 and 2), a single contour such as an airfoil in the physical plane (z -plane) was transformed into a single straight line contour (airfoil chord) in another plane (ζ -plane). The line in the ζ -plane is related to a circle in a third plane, the p -plane, by a known transformation that maps the unit circle with its center at the origin into the straight line such that the region outside the circle is mapped into the region outside the straight line. Because the contour in the z -plane also transforms into the same circle in the p -plane in such a manner that the regions exterior to the contours correspond, the function $z - \zeta$ is regular everywhere on and outside the circle in the p -plane. This vector difference $z - \zeta$ between conformally related points is called the Cartesian mapping function (CMF).

The real and imaginary parts of the CMF are denoted by Δx and Δy , respectively. Because of the regularity of the CMF outside the circle,

$$z - \zeta = \Delta x (\rho, \varphi) + i\Delta y (\rho, \varphi) = \sum_{n=0}^{\infty} C_{-n} p^{-n} \quad (1)$$

where

$$p = \rho e^{i\varphi}$$

$$C_{-n} = a_{-n} + i b_{-n}$$

On the circle $p = e^{i\varphi}$ the following relations hold:

$$\left. \begin{aligned} \Delta y (1, \varphi) &= \frac{1}{2\pi} \int_0^{2\pi} \Delta x (1, \varphi') \cot \frac{(\varphi' - \varphi)}{2} d\varphi' \\ \Delta x (1, \varphi) &= - \frac{1}{2\pi} \int_0^{2\pi} \Delta y (1, \varphi') \cot \frac{(\varphi' - \varphi)}{2} d\varphi' \end{aligned} \right\} \quad (2)$$

Equations (2) are the fundamental equations whereby the transformation between the z - and ζ -planes can be calculated.

The CMF for Two Contours

In general, two contours in the physical plane can be transformed into two straight-line contours in the ζ -plane. The lines in the ζ -plane can, in turn, be transformed into two concentric circles in the p -plane, whose centers are at the origin and whose radii are equal to 1 and q ($q < 1$). The transformation is such that the region between the two circles is transformed into the region between the contours.

In the case discussed in the present paper one of the contours in the z -plane is the airfoil itself; the other contour consists of the channel walls, both walls together being considered as one contour extending to infinity in two directions. The contours in the ζ -plane consist of a finite straight line into which the airfoil is transformed and a transformed channel whose walls are plane and parallel to the real axis. In the p -plane, the finite straight line, and hence the airfoil, are mapped into the outer circle whose radius is unity, and the channels of both the ζ - and the z -planes are mapped into the inner circle whose radius is q . Thus, as the outer circle is traced in a counterclockwise direction, the airfoil and the finite straight line are traced in a clockwise direction. In the same manner, as the inner circle is traced counterclockwise, the channel is traced clockwise.

As in the case of the single contour, the regions at infinity in the z - and ζ -planes correspond, but the vector difference $z - \zeta$ is regular on the boundary of both circles and within the annulus formed by them. As before, $z - \zeta$ is the CMF and Δx and Δy are its real and imaginary parts. Because of the regularity of $z - \zeta$ in the annulus, the CMF may be expanded as follows (cf. equation (1)):

$$z - \zeta = \Delta x (\rho, \varphi) + i\Delta y (\rho, \varphi) = \sum_{-\infty}^{\infty} C_n p^n \quad (3)$$

where

$$p = \rho e^{i\varphi}$$

$$C_n = a_n + ib_n$$

Inasmuch as the full Laurent series is used in equation (3), the relations between Δx and Δy on the two circles differ from the simple relations given by equations (2).

Appendix C of reference 2 provides relations between the components of the CMF on the two circles, but the expressions are not easily used for the purpose of calculation. More convenient relations have been derived in reference 3. Although the correct result

is obtained, the method of derivation is not fully given. The relations are derived in more detail in appendix A of the present paper. These relations between the components of the CMF are the following.

The subscripts 1 and 2 indicate the values of the CMF on the circle of unit radius and the circle of radius q , respectively. That is:

$$\left. \begin{aligned} \Delta x_1(\varphi) &= \Delta x(1, \varphi) \\ \Delta y_1(\varphi) &= \Delta y(1, \varphi) \\ \Delta x_2(\varphi) &= \Delta x(q, \varphi) \\ \Delta y_2(\varphi) &= \Delta y(q, \varphi) \end{aligned} \right\} \quad (4)$$

Then, as shown in appendix A:

$$\left. \begin{aligned} \Delta x_1(\varphi) &= a_0 + \frac{1}{\pi} \int_0^{2\pi} \Delta y_1(\varphi') \left[\frac{1}{2} \cot \frac{(\varphi' - \varphi)}{2} + \sum_{n=1}^{\infty} \frac{2q^{2n}}{1-q^{2n}} \sin n(\varphi' - \varphi) \right] d\varphi' \\ &\quad - \frac{1}{\pi} \int_0^{2\pi} \Delta y_2(\varphi') \sum_{n=1}^{\infty} \frac{2q^n}{1-q^{2n}} \sin n(\varphi' - \varphi) d\varphi' \\ \Delta x_2(\varphi) &= a_0 - \frac{1}{\pi} \int_0^{2\pi} \Delta y_2(\varphi') \left[\frac{1}{2} \cot \frac{(\varphi' - \varphi)}{2} + \sum_{n=1}^{\infty} \frac{2q^{2n}}{1-q^{2n}} \sin n(\varphi' - \varphi) \right] d\varphi' \\ &\quad + \frac{1}{\pi} \int_0^{2\pi} \Delta y_1(\varphi') \sum_{n=1}^{\infty} \frac{2q^n}{1-q^{2n}} \sin n(\varphi' - \varphi) d\varphi' \\ \Delta y_1(\varphi) &= b_0 - \frac{1}{\pi} \int_0^{2\pi} \Delta x_1(\varphi') \left[\frac{1}{2} \cot \frac{(\varphi' - \varphi)}{2} + \sum_{n=1}^{\infty} \frac{2q^{2n}}{1-q^{2n}} \sin n(\varphi' - \varphi) \right] d\varphi' \\ &\quad + \frac{1}{\pi} \int_0^{2\pi} \Delta x_2(\varphi') \sum_{n=1}^{\infty} \frac{2q^n}{1-q^{2n}} \sin n(\varphi' - \varphi) d\varphi' \\ \Delta y_2(\varphi) &= b_0 + \frac{1}{\pi} \int_0^{2\pi} \Delta x_2(\varphi') \left[\frac{1}{2} \cot \frac{(\varphi' - \varphi)}{2} + \sum_{n=1}^{\infty} \frac{2q^{2n}}{1-q^{2n}} \sin n(\varphi' - \varphi) \right] d\varphi' \\ &\quad - \frac{1}{\pi} \int_0^{2\pi} \Delta x_1(\varphi') \sum_{n=1}^{\infty} \frac{2q^n}{1-q^{2n}} \sin n(\varphi' - \varphi) d\varphi' \end{aligned} \right\} \quad (5)$$

and

$$\left. \begin{aligned} \int_0^{2\pi} \Delta x_1(\varphi) d\varphi &= \int_0^{2\pi} \Delta x_2(\varphi) d\varphi \\ \int_0^{2\pi} \Delta y_1(\varphi) d\varphi &= \int_0^{2\pi} \Delta y_2(\varphi) d\varphi \end{aligned} \right\} \quad (6)$$

The introduction of elliptic functions simplifies equations (5). The elliptic functions introduced at this point and used at other places in this paper are treated in various texts with varying notations. The notation used throughout this paper is that of Tannery and Molk (reference 5). From reference 5 (t. IV, p. 100), the following series for the \wp -functions are obtained:

$$\frac{1}{2\pi} \frac{\wp_1'(v)}{\wp_1(v)} = \frac{1}{2} \cot \pi v + \sum_{n=1}^{\infty} \frac{2q^{2n}}{1-q^{2n}} \sin 2\pi nv \quad (7)$$

$$\frac{1}{2\pi} \frac{\wp_4'(v)}{\wp_4(v)} = \sum_{n=1}^{\infty} \frac{2q^n}{1-q^{2n}} \sin 2\pi nv \quad (8)$$

Hence, from equation (5):

$$\Delta x_1(\varphi) = a_0 + \frac{1}{2\pi^2} \int_0^{2\pi} \Delta y_1(\varphi') \frac{\vartheta_1' \left(\frac{\varphi' - \varphi}{2\pi} \right)}{\vartheta_1 \left(\frac{\varphi' - \varphi}{2\pi} \right)} d\varphi'$$

$$- \frac{1}{2\pi^2} \int_0^{2\pi} \Delta y_2(\varphi') \frac{\vartheta_4' \left(\frac{\varphi' - \varphi}{2\pi} \right)}{\vartheta_4 \left(\frac{\varphi' - \varphi}{2\pi} \right)} d\varphi'$$

$$\Delta x_2(\varphi) = a_0 - \frac{1}{2\pi^2} \int_0^{2\pi} \Delta y_2(\varphi') \frac{\vartheta_1' \left(\frac{\varphi' - \varphi}{2\pi} \right)}{\vartheta_1 \left(\frac{\varphi' - \varphi}{2\pi} \right)} d\varphi'$$

$$+ \frac{1}{2\pi^2} \int_0^{2\pi} \Delta y_1(\varphi') \frac{\vartheta_4' \left(\frac{\varphi' - \varphi}{2\pi} \right)}{\vartheta_4 \left(\frac{\varphi' - \varphi}{2\pi} \right)} d\varphi'$$

(9)

$$\Delta y_1(\varphi) = b_0 - \frac{1}{2\pi^2} \int_0^{2\pi} \Delta x_1(\varphi') \frac{\vartheta_1' \left(\frac{\varphi' - \varphi}{2\pi} \right)}{\vartheta_1 \left(\frac{\varphi' - \varphi}{2\pi} \right)} d\varphi'$$

$$+ \frac{1}{2\pi^2} \int_0^{2\pi} \Delta x_2(\varphi') \frac{\vartheta_4' \left(\frac{\varphi' - \varphi}{2\pi} \right)}{\vartheta_4 \left(\frac{\varphi' - \varphi}{2\pi} \right)} d\varphi'$$

$$\Delta y_2(\varphi) = b_0 + \frac{1}{2\pi^2} \int_0^{2\pi} \Delta x_2(\varphi') \frac{\vartheta_1' \left(\frac{\varphi' - \varphi}{2\pi} \right)}{\vartheta_1 \left(\frac{\varphi' - \varphi}{2\pi} \right)} d\varphi'$$

$$- \frac{1}{2\pi^2} \int_0^{2\pi} \Delta x_1(\varphi') \frac{\vartheta_4' \left(\frac{\varphi' - \varphi}{2\pi} \right)}{\vartheta_4 \left(\frac{\varphi' - \varphi}{2\pi} \right)} d\varphi'$$

In the same way that the relations expressed by equations (2) are a limiting form of Poisson's integral, the integrals in equations (5) or (9) are limiting forms of Villat's analog to Poisson's integral. Villat's integral (reference 6) gives the value of a function within an annulus when the real part of the function is known on the bounding circles.

The relations expressed by equations (5) reduce to those expressed by equations (2) when the radius of the inner circle approaches zero; that is, when the channel walls move to infinity. The signs differ, however, because the CMF that is defined within the annulus in equations (5) is defined within the outer circle as the radius of the inner circle goes to zero, whereas, in the case of equations (2), the CMF is defined outside that circle.

The ζ -Plane and Its Transformation into the p-Plane

As already described, the ζ -plane contains a plane-walled channel within which there is a flat plate. The transformation mapping these contours into two concentric circles has been obtained by Tomotika (reference 7), who has also obtained the velocity potential for this case. Tomotika's results will be briefly presented and the form in which they are most useful in applying the CMF method will be given in more detail.

Let $\bar{\alpha}$ be the angle of attack of the flat plate. The transformation between the ζ -plane and the p-plane is shown in figure 1 and given mathematically as

$$\begin{aligned} \zeta = & -\frac{2h}{\pi} e^{i(\frac{\pi}{2}+\delta)} \sum_{n=1}^{\infty} \frac{q^n \sin n\varphi_2}{n(l + 2q^{2n} \cos 2\delta + q^{4n})} \\ & \times [p^n(e^{i\delta} + q^{2n}e^{-i\delta}) + p^{-n}(e^{-i\delta} + q^{2n}e^{i\delta})] + \tau \end{aligned} \quad (10)$$

or in another form

$$\begin{aligned} \zeta = & \frac{i2h}{\pi} \left\{ \frac{1}{2i} \log_e \frac{pqe^{i\varphi_2}}{pqe^{-i\varphi_2}} + \sum_{n=1}^{\infty} \frac{q^{2n} \sin n\varphi_2}{n(l-2q^{2n} \cos 2\bar{\alpha} + q^{4n})} \right. \\ & \left. \times \left[\left(\frac{p}{q} \right)^n \left(e^{-2i\bar{\alpha}} - q^{2n} \right) - \left(\frac{p}{q} \right)^{-n} \left(e^{2i\bar{\alpha}} - q^{2n} \right) \right] \right\} + \tau \end{aligned} \quad (11)$$

where h is the distance between the channel walls, $\delta = \frac{\pi}{2} - \bar{\alpha}$, and τ is a constant. The substitution of $p = e^{i\varphi}$ in equation (10) yields the equation of the flat plate; the substitution of $p = qe^{i\varphi}$ in equation (11) yields the equation of the channel walls, which are parallel to the real axis. The use of the two forms of the transformation simplifies the resulting equations in φ for the flat plate and channel walls.

Four values of the central angle φ ($\varphi_1, \varphi_2, \varphi_3$, and φ_4) are important in the mapping. From reference 7 the points $p = e^{i\varphi_1}, e^{i(2\pi-\varphi_1)}$, denoted by B and B' map into the stagnation points on the flat plate for zero circulation; the points $p = qe^{i\varphi_2}, qe^{i(2\pi-\varphi_2)}$, denoted by H and H' map into $\mp\infty$, respectively; the points $p = e^{i\varphi_3}, e^{i\varphi_4}$, denoted by A' and A , map into the extremities of the plate. The points are shown in figure 1.

The values of q and φ_2 in equations (9) and (10) are determined by the length of the plate, its position, and the various relations between the four special values of φ . From equation (10) or equation (11)

$$\varphi_3 + \varphi_4 = 2\bar{\alpha} \quad (12)$$

$$\frac{\vartheta_4'(\frac{\varphi_1+\varphi_2}{2\pi})}{\vartheta_4(\frac{\varphi_1+\varphi_2}{2\pi})} - \frac{\vartheta_4'(\frac{\varphi_1-\varphi_2}{2\pi})}{\vartheta_4(\frac{\varphi_1-\varphi_2}{2\pi})} = 0 \quad (13)$$

or

$$8\pi \sum_{n=1}^{\infty} \frac{q^n}{1-q^{2n}} \cos n\varphi_1 \sin n\varphi_2 = 0$$

$$\vartheta_4\left(\frac{\varphi_3-\varphi_2}{2\pi}\right) \vartheta_4\left(\frac{\varphi_4-\varphi_2}{2\pi}\right) = \vartheta_4\left(\frac{\varphi_3+\varphi_2}{2\pi}\right) \vartheta_4\left(\frac{\varphi_4+\varphi_2}{2\pi}\right) \quad (14)$$

$$\frac{L}{h} = \frac{8}{\pi} \sum_{n=1}^{\infty} \frac{q^n \sin n\varphi_2 \sin \frac{n(\varphi_3-\varphi_4)}{2}}{n(l-2q^{2n} \cos 2\bar{\alpha} + q^{4n})} [\cos(n-1) \bar{\alpha} - q^{2n} \cos(n+1) \bar{\alpha}] \quad (15)$$

$$\frac{d}{h} = \frac{1}{\pi} \left(\frac{\pi}{2} - \varphi_2 \right) + \frac{4}{\pi} \sin \bar{\alpha} \sum_{n=1}^{\infty} \frac{q^n \sin n\varphi_2 \cos \frac{n(\varphi_3 - \varphi_4)}{2}}{n(l - 2q^{2n} \cos 2\bar{\alpha} + q^{4n})} \\ \times [\sin(n-1) \bar{\alpha} - q^{2n} \sin(n+1)^2] \quad (16)$$

where L is the length of the plate and d is the vertical distance of the midpoint from the center line of the channel.

In order to find the values of q , φ_1 , φ_2 , φ_3 , and φ_4 for a given length and position of the plate, equations (12) to (16) should be solved simultaneously.

In principle, it is possible to transform the flat plate at any value of $\bar{\alpha}$ into the airfoil at angle of attack set at α . The value of $\bar{\alpha}$ is fixed at the value that accomplishes the transformation with the least labor. In the case to be calculated, $\bar{\alpha}$ is set equal to zero. For this value of $\bar{\alpha}$, Tomotika's formulas (reference 7) are considerably simplified. If the distance between the channel walls is taken as unity, the equations simplify as follows:

$$\zeta = \frac{2i}{\pi} \sum_{n=1}^{\infty} \frac{q^n \sin n\varphi_2}{n(l - q^{2n})} (p^n - p^{-n}) + \tau \quad (17)$$

or equivalently

$$\zeta = \frac{2i}{\pi} \left\{ \frac{1}{2i} \log_e \frac{p - q e^{i\varphi_2}}{p - q e^{-i\varphi_2}} + \sum_{n=1}^{\infty} \frac{q^{2n} \sin n\varphi_2}{n(l - q^{2n})} \left[\left(\frac{p}{q} \right)^n - \left(\frac{p}{q} \right)^{-n} \right] \right\} + \tau \quad (18)$$

and φ_2 can be found by using the equation

$$d = \frac{1}{2} - \frac{\varphi_2}{\pi} \quad (19)$$

The quantities q , φ_1 , φ_3 , and φ_4 may be found by solving simultaneously equations (12), (13), (14), and (15), which also become simpler than the equations for the general case. The constant τ may be restricted to real values, because it merely determines the position of the channel and the flat plate with respect to the axes in the ζ -plane.

A special case useful for numerical work is that for which $d = 0$. For this position of the flat plate $\varphi_1 = \varphi_2 = \varphi_3 = -\varphi_4 = \pi/2$ and

$$L = \frac{8}{\pi} \sum_{n=1}^{\infty} \frac{q^{2n-1}}{(2n-1)[1-q^{2(2n-1)}]} \quad (20)$$

Hence, q can be found from equation (20) alone when the length of the plate is prescribed.

If ζ is separated into its real and imaginary parts, $\zeta = \xi + i\eta$, ξ and η can be found as functions of φ . The equation of the flat plate is found by setting $p = e^{i\varphi}$ in equation (17). Then, when the subscripts 1 and 2 denote the values of the function on the plate and on the channel, respectively,

$$\xi_1 = -\frac{4}{\pi} \sum_{n=1}^{\infty} \frac{q^n \sin n\varphi_2}{n(1-q^{2n})} \sin n\varphi + \tau \quad (21)$$

$$\eta_1 = 0 \quad (22)$$

Thus the flat plate lies on the real axis of the ζ -plane. The equation of the channel walls is found by setting $p = qe^{i\varphi}$ in equation (18). Then

$$\xi_2 = \frac{1}{\pi} \left\{ \log_e \left| \frac{\sin \frac{1}{2}(\varphi-\varphi_2)}{\sin \frac{1}{2}(\varphi+\varphi_2)} \right| - 4 \sum_{n=1}^{\infty} \frac{q^{2n} \sin n\varphi_2}{n(1-q^{2n})} \sin n\varphi \right\} + \tau \quad (23)$$

$$\begin{aligned} \eta_2 &= \frac{\varphi_2}{\pi} = \frac{1}{2} - d && (2\pi - \varphi_2 > \varphi > \varphi_2) \\ \eta_2 &= \frac{\varphi_2}{\pi} - 1 = -\left(\frac{1}{2} + d\right) && (\varphi_2 > \varphi > -\varphi_2) \end{aligned} \quad \left. \right\} \quad (24)$$

Airfoil Position and Adjustments in Terms of the CMF

The z -plane and the ζ -plane are shown superimposed in figure 2 in which the geometric meaning of the CMF is also indicated. If the abscissas and ordinates of the airfoil are denoted by x_1 , y_1 and the abscissas and ordinates of the channel walls by x_2 , y_2 , the definition of the CMF shows that

$$\left. \begin{aligned} x_1(\varphi) &= \xi_1(\varphi) + \Delta x_1(\varphi) \\ y_1(\varphi) &= \Delta y_1(\varphi) \\ x_2(\varphi) &= \xi_2(\varphi) + \Delta x_2(\varphi) \\ y_2(\varphi) &= \eta_2 + \Delta y_2(\varphi) \end{aligned} \right\} \quad (25)$$

In order to determine the constants q and φ_2 that appear explicitly in the expressions for ξ and η and also the angles φ_N and φ_T that correspond to the leading and trailing edges of the airfoil, the airfoil is placed in a normal position with respect to the y axis. If c is the chord of the airfoil and α is the angle of attack, the normal position is given by

$$\left. \begin{aligned} x_1(\varphi_N) &= -\frac{c}{2} \cos \alpha \\ x_1(\varphi_T) &= \frac{c}{2} \cos \alpha \end{aligned} \right\} \quad (26)$$

From equations (25) and (26), the following formula is obtained:

$$\xi_1(\varphi_T) - \xi_1(\varphi_N) = c \cos \alpha - \Delta x_1(\varphi_T) + \Delta x_1(\varphi_N) \quad (27)$$

The angles φ_N and φ_T corresponding to leading and trailing edges are obtained from the condition of a maximum for the abscissa $x_1(\varphi)$,

$$\frac{dx_1(\varphi_N)}{d\varphi} = 0 \quad \frac{dx_1(\varphi_T)}{d\varphi} = 0 \quad (28)$$

or, by equations (20) and (24),

$$\frac{d\Delta x_1(\varphi)}{d\varphi} = \frac{4}{\pi} \sum_{n=1}^{\infty} \frac{q^n \sin n\varphi_2}{1 - q^{2n}} \cos n\varphi \quad (29)$$

for $\varphi = \varphi_N$ or φ_T .

The value of φ_2 , or what is equivalent the value of d , is found from

$$\int_0^{2\pi} \Delta y_1(\varphi) d\varphi = \int_0^{2\pi} \Delta y_2(\varphi) d\varphi \quad (6)$$

as follows: Let $r(\varphi)$ denote the value of the ordinate of the airfoil measured from the center line of the channel in the ζ -plane. From the definition

$$r(\varphi) = \Delta y_1(\varphi) + d \quad (30)$$

Hence, using equation (6),

$$d = \frac{1}{2\pi} \int_0^{2\pi} r(\varphi) d\varphi - \frac{1}{2\pi} \int_0^{2\pi} \Delta y_2(\varphi) d\varphi \quad (31)$$

and φ_2 is obtained from equation (19).

The constant τ is obtained by adding the equations of (26). The resulting formula is

$$\tau = \frac{4}{\pi} \sum_{n=1}^{\infty} \frac{q^n \sin n\varphi_2}{n(1-q^{2n})} \sin \frac{n(\varphi_N+\varphi_T)}{2} \cos \frac{n(\varphi_N-\varphi_T)}{2} - \frac{\Delta x_1(\varphi_N) + \Delta x_1(\varphi_T)}{2} \quad (32)$$

These equations completely determine the constants q , τ , φ_N , φ_T , and φ_2 in terms of the CMF. The value of φ_2 is calculated from equations (31) and (19); the use of this value in equations (27) and (29) permit these equations to be solved simultaneously for q , φ_N , φ_T ; and finally τ can be determined from equation (32).

Velocity Distribution on the Airfoil

and on the Channel Walls

The complex velocity potential W , derived from the results of reference 7, is

$$W = \frac{Vh}{\pi} \log_e \frac{\vartheta_4\left(\frac{i \log_e p + \varphi_2}{2\pi}\right) \vartheta_4\left(\frac{\varphi_1 + \varphi_2}{2\pi}\right)}{\vartheta_4\left(\frac{i \log_e p - \varphi_2}{2\pi}\right) \vartheta_4\left(\frac{\varphi_1 - \varphi_2}{2\pi}\right)} - \frac{i\Gamma}{2\pi} \log_e p \quad (33)$$

where V is the velocity at infinity and Γ is the circulation.

The velocity distribution on the airfoil and on the channel walls is obtained from the velocity potential given by equation (33). The formula for the velocity in the z -plane is

$$v_z = \left| \frac{dW}{dp} \right| \quad (34)$$

On the airfoil, from equations (8) and (33)

$$\left(\frac{dW}{dp} \right)_{p=e^{i\varphi}} = \frac{ie^{-i\varphi}}{2\pi} \left[\left(8V \sum_{n=1}^{\infty} \frac{q^n \sin n\varphi_2}{1-q^{2n}} \cos n\varphi \right) - \Gamma \right] \quad (35)$$

The circulation Γ in equation (35) is adjusted to satisfy the Kutta condition at the trailing edge of the airfoil $\left(\frac{dW}{dp} \right)_{\varphi=\varphi_T} = 0$. The result is

$$\Gamma = 8V \sum_{n=1}^{\infty} \frac{q^n \sin n\varphi_2}{1-q^{2n}} \cos n\varphi_T \quad (36)$$

Also

$$\begin{aligned} \left(\frac{dz}{dp} \right)_{p=e^{i\varphi}} &= \left(\frac{d\zeta}{dp} \right)_{p=e^{i\varphi}} - i \frac{d\Delta x_1}{d\varphi} e^{-i\varphi} + \frac{d\Delta y_1(\varphi)}{d\varphi} e^{-i\varphi} \\ &= \frac{4ie^{-i\varphi}}{\pi} \sum_{n=1}^{\infty} \frac{q^n \sin n\varphi_2}{1-q^{2n}} \cos n\varphi - \frac{id\Delta x_1(\varphi)}{d\varphi} e^{-i\varphi} \\ &\quad + \frac{d\Delta y_1(\varphi)}{d\varphi} e^{-i\varphi} \end{aligned} \quad (37)$$

Hence, the velocity distribution on the airfoil is

$$\frac{v_{cl}}{V} = \frac{\frac{4}{\pi}}{\sqrt{1 + \left[\left(\frac{4}{\pi} \sum_{n=1}^{\infty} \frac{q^n \sin n\varphi_2}{1-q^{2n}} \cos n\varphi - \frac{d\Delta x_1(\varphi)}{d\varphi} \right)^2 + \left(\frac{d\Delta y_1(\varphi)}{d\varphi} \right)^2 \right]}} \quad (38)$$

where v_{cl} has been written for v_z .

The velocity distribution on the channel walls is found by replacing p by $qe^{i\varphi}$ in equation (33). The substitution results in

$$\left(\frac{dw}{dp} \right)_{p=qe^{i\varphi}} = iq^{-1} e^{-i\varphi} V \left(\frac{1}{\pi} \frac{\sin \varphi_2}{\cos \varphi - \cos \varphi_2} + \frac{4}{\pi} \sum_{n=1}^{\infty} \frac{q^{2n} \sin n\varphi_2 \cos n\varphi}{1-q^{2n}} - \frac{\Gamma}{2\pi V} \right) \quad (39)$$

where Γ has the value given by equation (36).

Also

$$\begin{aligned}
 \left(\frac{dz}{dp} \right)_{p=qe^{i\psi}} &= \left(\frac{d\zeta}{dp} \right)_{p=qe^{i\psi}} - iq^{-1}e^{-i\phi} \frac{d\Delta x_2(\phi)}{d\phi} + q^{-1}e^{-i\phi} \frac{d\Delta y_2(\phi)}{d\phi} \\
 &= iq^{-1}e^{-i\phi} \frac{1}{\pi} \frac{\sin \Phi_2}{\cos \Phi - \cos \Phi_2} + \frac{4}{\pi} iq^{-1}e^{-i\phi} \sum_{n=1}^{\infty} \frac{q^{2n} \sin n\Phi_2}{1-q^{2n}} \cos n\phi - iq^{-1}e^{-i\phi} \frac{d\Delta x_2(\phi)}{d\phi} + q^{-1}e^{-i\phi} \frac{d\Delta y_2(\phi)}{d\phi} \\
 \end{aligned} \tag{40}$$

Hence, the velocity distribution on the channel walls is given by

$$\frac{v_{c2}}{V} = \frac{\left| \frac{\sin \Phi_2}{\pi(\cos \Phi - \cos \Phi_2)} + \frac{4}{\pi} \sum_{n=1}^{\infty} \frac{q^{2n} \sin n\Phi_2}{1-q^{2n}} \cos n\phi - \frac{\Gamma}{2\pi V} \right|^2}{\left[\frac{\sin \Phi_2}{\pi(\cos \Phi - \cos \Phi_2)} + \frac{4}{\pi} \sum_{n=1}^{\infty} \frac{q^{2n} \sin n\Phi_2}{1-q^{2n}} \cos n\phi - \frac{d\Delta x_2(\phi)}{d\phi} + \frac{d\Delta y_2(\phi)}{d\phi} \right]^2} \tag{41}$$

Lift on the Airfoil in the Channel

The lift on the airfoil in the channel can be found by evaluating a modified form of Blasius' integral in the p -plane. The expression for the lift involves the CMF and the radius of the inner circle; that is, the lift depends on the shape and the position of the airfoil and on the shape of the channel walls as well as on the circulation. This dependence is in contrast to the case of the isolated airfoil, in which the lift on any body is the same for a fixed circulation. The dependence of lift upon the airfoil shape for the case of the airfoil in a plane-walled channel has also been shown by Havelock (reference 8) who finds the potential function directly without the use of conformal mapping.

The expression for the lift is too complicated for numerical calculation. A more convenient way of obtaining the lift is to integrate the pressure distribution on the airfoil or the pressure distribution on the walls.

Method of Successive Approximations for Obtaining CMF

The CMF can now be calculated for a given configuration by a method of successive approximation analogous to that of reference 2.

1. The airfoil and the channel walls are drawn such that the airfoil is in the normal position, as shown in figure 2. The center line of the channel in the ζ -plane is located on the figure in order that the airfoil ordinates $r(\varphi)$ may be read. The scale is so chosen that the distance between the channel walls in the ζ -plane is unity.

2. From a previous approximation, approximate values of q , T , φ_2 , φ_N , and φ_T are known, as well as approximate values of the abscissas $x_1(\varphi)$ and $x_2(\varphi)$ at a convenient set of values of φ from 0 to 2π radians. Through the use of the known values of $x_1(\varphi)$, $r(\varphi)$ is measured. A set of values of $\Delta y_2(\varphi)$ are also measured through the use of the known values of $x_2(\varphi)$. A value of d and a new value of φ_2 are obtained from equations (31) and (19).

If no better values are available, the initial approximation for $x_1(\varphi)$ and $x_2(\varphi)$ may be that obtained for the flat plate situated along the center line of a plane-walled channel. In this case x_1 and x_2 are given by equations (21) and (23) for ξ_1

and ξ_2 . The value of q is obtained from equation (20), where L is replaced by $c \cos \alpha$. Both φ_2 and φ_N equal $\pi/2$ and φ_T equals $3\pi/2$. The constant τ equals zero.

3. The functions Δx_1 and Δx_2 are calculated by means of the first and second equations of (5). The value of q used is the approximate value of step 2. The numerical details of the calculation are given in appendix B.

4. New values of φ_N , φ_T , and q are obtained by solving equations (27) and (29) simultaneously for these quantities.

An alternative method of determining φ_N , φ_T , and q is a purely graphical one. The approximate function $x_1(\varphi)$, which is also a function of q , is plotted against φ in the regions of the extreme values of x_1 . From this graph φ_N and φ_T are determined. These values are substituted in equation (27), from which a new value of q is obtained that is used to re-evaluate x_1 . The procedure is continued until sufficient accuracy is obtained. Finally τ is calculated from equation (32).

5. A new set of values for $x_1(\varphi)$ and $x_2(\varphi)$ are calculated using the new values of the constants and the values of Δx_1 and Δx_2 calculated in step 3.

Steps 2 through 5 are repeated until a plot of $y(\varphi)$ against $x(\varphi)$ for both the airfoil and the channel walls yield shapes that are as close as desired to the shapes plotted in step 1.

If the walls of the channel in the z -plane are flat, $\Delta y_2(\varphi)$ is set equal to zero, and a considerable simplification in the numerical procedure results. This case is the most common and the method is not at all difficult to apply. The discussion of numerical results will provide an idea of the actual work involved.

After the components of the CMF and the various constants have been evaluated by the method of iteration just described, the velocity distribution may be found from equations (38) and (41) for the airfoil and for the channel walls, respectively. The derivatives of the CMF in the formulas for the velocity distribution were measured in the cases calculated; although an expression exists that gives the values of the derivative in terms of the CMF as in reference 1, it is too cumbersome to use.

ILLUSTRATIVE EXAMPLES USING CONFORMAL MAPPING

The method of conformal mapping outlined has been applied to the 12-percent symmetrical airfoil treated in reference 1. The ordinates of this airfoil are given in table 1 and the airfoil shape is shown in the figures in which the velocity distributions are plotted. For the calculations of the present paper the airfoil was assumed to be placed at the center of a plane-walled channel. The chord to height (c/h) ratio was taken to be 0.5. Velocity corrections were calculated for angles of attack of 0° and 4° .

For the case of $\alpha = 0^\circ$ the range of φ from 0 to 2π radians was divided into 24 equal intervals. Two approximations, starting from the $x(\varphi)$ of the flat plate, were necessary for the derived airfoil contour to coincide with the given contour for a scale of chord length of 20 inches and ordinate scale five times that of the abscissa scale. In no case were more than six terms used in any of the infinite series in the preceding formulas, for the series converge rapidly. The velocity distribution for the case of $\alpha = 0^\circ$ is shown in figure 3. The velocity distribution on the walls of the channel is included in the figure and is drawn to a scale five times as large as the scale for the velocity distribution on the airfoil. The CMF together with the velocity distribution is given in table 2. The velocity distribution on the airfoil for this case had been previously calculated by the method of finite chord in reference 1. The results are compared in figure 4 and are in close agreement, which indicates that the numerical methods used in both processes were sufficiently accurate.

The velocity distribution for the case of angle of attack of 4° is plotted in figure 5. Figure 6 shows for the purpose of comparison the velocity distribution for the airfoil in the free stream at $\alpha = 4^\circ$. In this case four approximations, starting from the flat plate, were necessary to obtain coincidence between the derived airfoil and the given airfoil to the same ordinate and abscissa scale as in the case of $\alpha = 0^\circ$. In the first three approximations the φ range was divided into 24 equal intervals, but in the fourth approximation the length of the intervals was halved so that the CMF was evaluated at 48 points. The mapping data and velocity distribution are given in table 3; the nature of the CMF is shown by figure 7 where the component functions are plotted. The velocity distribution for the airfoil in the free stream was obtained by the method of reference 2.

The velocity correction for the airfoil at an angle of attack of 0° was discussed in reference 1. The velocity corrections for the airfoil at the angle of attack of 4° are plotted in figure 8.

The irregularities of the correction are due to local curvature fluctuations of the airfoil surface and correspond to the irregularities found in the corrections for the same airfoil at $\alpha = 0^\circ$. (See reference 1.)

The velocity corrections are positive on the upper surface of the airfoil but are for the most part very nearly zero on the lower surface. This behavior of the correction indicates that the lift on the airfoil in the channel is greater than that on the airfoil in the free stream. The increase in lift has been shown by other authors through the use of approximate methods (see references 4, 7, 8, and 9) and will be further discussed.

The influence of the airfoil on the velocity distribution on the channel walls is shown in figures 3 and 5. The velocity distribution on the walls is very sensitive to the angle of attack. When the angle of attack is 0° (fig. 3) the nondimensional velocity on both the walls is greater than unity. The velocity rapidly approaches unity both upstream and downstream of the airfoil until at 1.75 chord lengths upstream and downstream of the origin the velocity has decreased from its maximum value 1.03 to substantially the value 1.0.

In contrast, when the angle of attack is 4° (fig. 5), the velocity is less than unity on the lower wall, and on the upper wall the velocity markedly increases over the velocity for the case of $\alpha = 0^\circ$. The maximum velocity on the upper wall moves forward toward the position at which the airfoil approaches closest to the wall; at the same time the minimum value on the lower wall is located at the position near the leading edge where the zero streamline rises to meet the airfoil at the stagnation point. On both the upper and lower walls the velocity approaches unity less rapidly than in the case of $\alpha = 0^\circ$. On the upper wall the maximum velocity is 1.095; the velocity 1.75 chord lengths upstream of the origin is 1.013; the velocity 1.75 chord lengths downstream is 1.010. On the lower wall the minimum velocity is 0.965; the velocity 1.75 chord lengths both upstream and downstream is 0.990.

APPROXIMATE VELOCITY CORRECTIONS FOR AN AIRFOIL PLACED

ALONG CENTER LINE OF A PLANE-WALLED CHANNEL

If an airfoil is placed midway between the walls of a plane-walled channel, simple approximate velocity corrections may be derived under the conditions that the angle of attack is small and that the thickness, chord, and camber are small in comparison with

the dimensions of the channel. Two such corrections will be explained. Both corrections depend upon the successive reflection of the airfoil in the channel walls by which a cascade of airfoils alternately upright and inverted is obtained. As is well known (see reference 9), the flow through such a cascade is equivalent to the flow about the airfoil in the plane-walled channel. In the first-order approximate theory, the image airfoils are replaced by doublets and by vortices; in the more elaborate treatment developed by Goldstein (reference 4), higher-order singularities are included. Inasmuch as the method of conformal mapping developed in the present paper is applied numerically to a symmetrical airfoil at the center of the channel, the approximate theories will be quantitatively discussed only for such airfoils. A more general treatment would follow along similar lines.

First-Order Theory

In the development of the first-order theory the vortex and the doublet are assumed to contribute independently to the velocity correction. The effect of the image vortices is to curve the stream and to increase the effective angle of attack and lift on the airfoil in the channel. The image doublets increase the velocity at the center of the channel and thus take into account the constricting effect of the channel walls. Glauert (reference 9, p. 49) obtained a formula for the ratio of the lift in the free stream to the lift in the channel. If it is assumed that the vortices merely change the angle of attack, the Kutta condition combined with Glauert's formula yields the following result:

$$\frac{\sin \alpha}{\sin \alpha_1} = 1 - \frac{\pi^2}{24} \left(\frac{c}{h} \right)^2 \quad (42)$$

where α is, as before, the angle of attack with respect to the direction of the flow at infinity and α_1 is the effective angle of attack due to the curved stream.

The increase of velocity at the center of the channel induced by the image doublets is assumed to be that due to the airfoil at its angle of zero lift. If this increase is denoted by u and, as before, V is the velocity at infinity in the channel, the following relation is true:

$$\frac{u}{V} = \frac{\pi^2}{12} \lambda \left(\frac{t}{h} \right)^2 \quad (43)$$

where for symmetrical airfoils

$$\lambda = \frac{4}{\pi} \frac{c}{t} \int \frac{v_c'}{V} \frac{y}{t} d\left(\frac{s}{c}\right) \quad (44)$$

as in reference 9 (p. 55). Here v_c' is the velocity on the airfoil when the airfoil is in the channel at an angle of attack of 0° and y is the distance to the upper surface of the airfoil measured normally from the chord line. The integral in equation (44) is taken with respect to the surface distance s along the upper surface of the airfoil from leading to trailing edge.

In the calculation of the strength of a doublet that is to replace an isolated airfoil, v_i rather than v_c' should be used. However, inasmuch as the strength of the doublet must be increased when it is used to replace the same airfoil in cascade, the use of v_c' , which is greater than v_i , will change the value of λ in the right direction.

The velocity correction is defined as

$$\frac{\Delta v}{V} = \left(\frac{v_c}{V} \right)_{\alpha_1} - \left(\frac{v_i}{V} \right)_\alpha \quad (45)$$

where $\left(\frac{v_c}{V} \right)_{\alpha_1}$ is the velocity on the airfoil in the channel expressed as a fraction of the ultimate upstream velocity when the airfoil is at an effective angle of attack α_1 and where $\left(\frac{v_i}{V} \right)_\alpha$ is the isolated airfoil velocity for the angle of attack α . Since the airfoil is small compared with the breadth of the channel, the flow about the airfoil in the channel is equivalent to the flow about an airfoil at an angle of attack α_1 in a free stream whose velocity at a great distance away is $V + u$. Therefore the following relation is true

$$\left(\frac{v_c}{V+u} \right)_{\alpha_1} = \left(\frac{v_i}{V} \right)_{\alpha_1} \quad (46)$$

or

$$\left(\frac{v_c}{V} \right)_{\alpha_1} = \left(\frac{v_i}{V} \right)_{\alpha_1} \left(1 + \frac{u}{V} \right) \quad (47)$$

The result is that

$$\frac{\Delta v}{V} = \left(\frac{v_i}{V} \right)_{\alpha_1} - \left(\frac{v_i}{V} \right)_\alpha + \left(\frac{v_i}{V} \right)_{\alpha_1} \frac{u}{V} \quad (48)$$

The formula for the velocity correction shows the importance of the changed angle of attack, for one part of the correction is the difference in the isolated airfoil velocity distributions at angles of attack α and α_1 ; the other term of the correction is proportional to the isolated velocity distribution at the increased angle of attack.

The correction obtained by the use of vortices and doublets is valid to the first order in $(\frac{c}{h})^2$ and tc/h^2 . When the angle of attack is 0° , the parameter $(\frac{c}{h})^2$ does not appear (reference 1).

Goldstein's Second-Order Velocity Correction

Goldstein (reference 4) first replaces the image airfoils by the doublet, the vortex, and the higher-order singularities given by the potential function of the airfoil in a uniform free stream. The nonuniform disturbance velocity produced by these singularities in the physical region, in particular at the location of the physical airfoil, is calculated, taking into account the change in direction of the stream. This first approximation nonuniform disturbance velocity (a) changes the velocity distribution on the airfoil from its isolated free-stream value and (b) changes the value of the singularities that are to be imaged. Change (b) is evaluated and a second approximation nonuniform distribution of the airfoil in the final nonuniform stream is calculated.

In principle, Goldstein's method is capable of yielding to any degree of accuracy the effect of a plane-walled channel on the two-dimensional velocity distribution of an arbitrary airfoil, arbitrarily situated. The successive approximations become increasingly laborious, however, and only the second-approximation formulas are given in reference 4.

The second-approximation formula for the constriction correction for the symmetrical airfoil situated in the center of the channel at a small angle of attack is obtained as:

$$\frac{v_c}{v_i} = \frac{(U)}{(V)} \frac{[P(\theta) - P(\pi) + \sin(\theta + \alpha_1) + \sin \alpha_1]}{[\sin(\theta + \alpha) + \sin \alpha]} \quad (49)$$

so that

$$\frac{\Delta v}{V} = \frac{v_i}{V} \left(\frac{v_c}{v_i} - 1 \right) \quad (50)$$

where U here represents the sum of the ultimate upstream velocity and the velocity at the center of the channel induced by the singularities so that $\frac{U}{V} - 1$ corresponds to u/V of the first-order theory; α_1 is, as in the previous approximate theory, an effective angle of attack with respect to the direction of the stream; the function $P(\theta)$ is a measure of the distortion of the stream caused by the singularities.

The Goldstein second-order image correction is accurate to the orders $(\frac{c}{h})^2$, $\frac{tc}{h^2}$, $(\frac{t}{h})^2$, $(\frac{c}{h})^4$, $\frac{c^3 t}{h^4}$, $\frac{c^2 t^2}{h^4}$, $\frac{ct^3}{h^4}$, and $(\frac{t}{h})^4$. When the angle

of attack is zero, the terms $(\frac{c}{h})^2$, $(\frac{t}{h})^2$, $(\frac{c}{h})^4$, and $(\frac{t}{h})^4$ do not appear.

Discussion of Numerical Results

of Approximate Theories

The first-order and second-order corrections were calculated for the 12-percent-thick symmetrical airfoil. The corrections for the airfoil at zero lift have been discussed in reference 1. The results for the angle of attack of 4° are plotted in figure 8. The constants used in the first-order correction are

λ	u/V	α_1
3.93	0.0116	4.459°

Those for the second-order correction are

c_0	c_1	c_2	c_3	c_4	α_1	$\frac{U}{V} - 1$
0.08722	0.05534	-0.02401	0.00455	0.00475	4.200°	0.0108

The first-order theory yields good results for the upper surface of the airfoil in that the correction so derived shows the same over-all trend as the correction obtained by conformal mapping. The approximate correction appears to be a mean curve to which are added components due to the curvature of the airfoil. For the lower surface, the approximate correction is not quite so good a mean line as it is for the upper surface. For both upper and lower surfaces, the contribution to the velocity correction due to the doublets and that due to the change in angle of attack are equally effective in forming the total correction.

For the upper surface of the airfoil, the Goldstein second-order image correction follows the same trend as the first-order image correction, but the values are more nearly constant. The second-order correction for the lower surface follows more closely the trend of the mapping correction than the first-order correction. From this example, the second-order correction appears to be more accurate than the first-order correction.

The incremental velocities u/V and $\frac{U}{V} - 1$ of the first- and second-order corrections, respectively, are in good agreement but the values of the effective angles of attack α_l' differ markedly. This difference accounts for the difference in the nature of the correction curve of figure 8 near the leading edge of the airfoil.

CALCULATION OF LIFT AND MOMENT

For the case of angle of attack of 4° , the lift coefficient c_l' for the airfoil in the channel was calculated by integrating the pressure distribution about the airfoil. The calculation for c_l' was also carried out by means of the two approximate theories.

The isolated airfoil lift coefficient c_l was 0.478. The value of c_l' obtained by the integration of the pressure distribution is 0.537; that value obtained from the second-order theory, 0.522 by the formulas of reference 4; and that value obtained from reference 9 (p. 49), 0.532. All the values of c_l' obtained indicate the expected increase in lift for the airfoil in the channel, and also show good agreement among themselves in that they do not vary more than 3 percent. The lift-coefficient correction, $c_l' - c_l$, varies, however, about 30 percent among the different theories.

The lift coefficient c_l' was also calculated by integrating the pressure distribution on the walls of the channel. Theoretically, the integration should be carried out to infinity on either side of

the airfoil. The practical calculation is, of course, impossible. The integration is therefore carried out only over a finite range to yield the lift coefficient c_l'' , and a correction factor used to take into account the effect of the rest of the channel.

The correction factor η , which is equal to c_l''/c_l' , has been derived in an approximate form in the appendix of reference 10. The airfoil is replaced by a row of vortices, which are imaged in the walls of the channel. The η factor for an individual vortex is calculated. The final η factor is obtained by averaging η for each vortex with a loading derived from thin airfoil theory as a weighting factor.

In figure 9 the lift coefficient c_l'' is plotted as a function of the limits of integration, which were taken symmetrically about the origin. The value of c_l'' , obtained by integrating the pressure distribution 1.75 chord lengths upstream and downstream of the origin, is 0.493. When this value is divided by the value of c_l' , derived by integrating the pressure distribution on the airfoil, a value η of 0.918 is obtained. The value of η obtained by the method of reference 10 is 0.900. The value of c_l' , obtained from the approximate value of η , is 0.548. The correction factor obtained by the approximate method is satisfactory to the order of the approximate theories previously discussed.

It is also possible to obtain the moment on the airfoil about any point by integrating the moment of the pressure (accurately calculated) on each element of area on the channel walls. A factor analogous to the η factor can be so determined that the integration for the moment over a finite range may be extended to take into account the regions on the channel walls a great distance away.

CONCLUSIONS

The analysis and numerical calculations of the present paper lead to the following conclusions:

1. The method of conformal transformation by means of the Cartesian mapping function provides a satisfactory numerical solution to the problem of obtaining the local velocity corrections for an arbitrary airfoil in a channel for the case of two-dimensional frictionless incompressible flow.
2. If closeness to the velocity corrections obtained by conformal mapping is used as a criterion, the second-order Goldstein

correction is more accurate than the first-order image vortex and doublet correction for thin airfoils at small angles of attack in giving velocity corrections in the examples calculated.

3. If it is necessary to obtain a higher-order correction than the second, the method of the Cartesian mapping function is probably more convenient to use than the Goldstein type correction.

4. The channel lift coefficients obtained by the two approximate theories are in good agreement with the lift obtained from the mapping velocity distribution; the lift corrections obtained by the two approximate theories are not in good agreement with the correction obtained by mapping results.

5. The existing method of finding the lift coefficients from the velocity distribution on the channel walls has been satisfactorily checked.

Aircraft Engine Research Laboratory,
National Advisory Committee for Aeronautics,
Cleveland, Ohio, December 4, 1946.

APPENDIX A

DERIVATION OF THE RELATIONS BETWEEN THE REAL
AND IMAGINARY PARTS OF THE CMF

Inasmuch as the CMF $z - \zeta$ is regular within the annulus and also on the bounding circles in the p -plane, it may be expanded in a Laurent series, which is valid in the annulus and on the circles bounding the annulus. Thus

$$z - \zeta = \Delta x(p, \varphi) + i\Delta y(p, \varphi) = \sum_{-\infty}^{\infty} C_n p^n \quad (A1)$$

From equation (A1) the following expressions are obtained:

$$\left. \begin{aligned} \Delta x_1(\varphi) &= a_0 + \sum_{1}^{\infty} (a_n + a_{-n}) \cos n\varphi - \sum_{1}^{\infty} (b_n - b_{-n}) \sin n\varphi \\ \Delta y_1(\varphi) &= b_0 + \sum_{1}^{\infty} (a_n - a_{-n}) \sin n\varphi + \sum_{1}^{\infty} (b_n + b_{-n}) \cos n\varphi \\ \Delta x_2(\varphi) &= a_0 + \sum_{1}^{\infty} (a_n q^n + a_{-n} q^{-n}) \cos n\varphi - \sum_{1}^{\infty} (b_n q^n - b_{-n} q^{-n}) \sin n\varphi \\ \Delta y_2(\varphi) &= b_0 + \sum_{1}^{\infty} (a_n q^n - a_{-n} q^{-n}) \sin n\varphi + \sum_{1}^{\infty} (b_n q^n + b_{-n} q^{-n}) \cos n\varphi \end{aligned} \right\} \quad (A2)$$

The values of a_n and b_n can be found by means of Fourier's rule in terms of the CMF.

When a_0 and b_0 are evaluated, the conditions of consistency that are necessary conditions for the regularity of the CMF in the annulus appear as

$$\left. \begin{aligned} 2\pi a_0 &= \int_0^{2\pi} \Delta x_1(\varphi) d\varphi = \int_0^{2\pi} \Delta x_2(\varphi) d\varphi \\ 2\pi b_0 &= \int_0^{2\pi} \Delta y_1(\varphi) d\varphi = \int_0^{2\pi} \Delta y_2(\varphi) d\varphi \end{aligned} \right\} \quad (A3)$$

Four relations are desired: Δx_1 and Δx_2 expressed in terms of Δy_1 and Δy_2 and, conversely, Δy_1 and Δy_2 expressed in terms of Δx_1 and Δx_2 . The derivation of the expression for Δy_1 in terms of Δx_1 and Δx_2 will now be carried out. The other relations will follow analogously.

Through the use of the first and third equations of (A2) and through the use of Fourier's rule, the coefficients a_n and b_n are evaluated. As a result of the calculation, the following equations are obtained:

$$\left. \begin{array}{l} a_n = \frac{-D_1 q^{-n} + D_2}{q^n - q^{-n}} \\ b_n = \frac{K_1 q^{-n} - K_2}{q^n - q^{-n}} \end{array} \right\} \quad \begin{array}{l} a_{-n} = \frac{D_1 q^n - D_2}{q^n - q^{-n}} \\ b_{-n} = \frac{K_1 q^n - K_2}{q^n - q^{-n}} \end{array} \quad (A4)$$

where

$$\left. \begin{array}{l} D_1 = \frac{1}{\pi} \int_0^{2\pi} \Delta x_1(\varphi) \cos n\varphi d\varphi \\ D_2 = \frac{1}{\pi} \int_0^{2\pi} \Delta x_2(\varphi) \cos n\varphi d\varphi \end{array} \right. \quad \left. \begin{array}{l} K_1 = \frac{1}{\pi} \int_0^{2\pi} \Delta x_1(\varphi) \sin n\varphi d\varphi \\ K_2 = \frac{1}{\pi} \int_0^{2\pi} \Delta x_2(\varphi) \sin n\varphi d\varphi \end{array} \right\} \quad (A5)$$

The values of the coefficients a_n and b_n are substituted in the infinite series expression for Δy_1 given by equations (A2). The values for K_1 , K_2 , D_1 , and D_2 as given by equations (A5) are also used. Thus

$$\Delta y_1(\varphi) = b_0 + \frac{1}{\pi} \sum_{n=1}^{\infty} \frac{q^n + q^{-n}}{q^n - q^{-n}} \int_0^{2\pi} \Delta x_1(\varphi') (\sin n\varphi' \cos n\varphi - \cos n\varphi' \sin n\varphi) d\varphi'$$

$$+ \frac{1}{\pi} \sum_{n=1}^{\infty} \frac{2}{q^n - q^{-n}} \int_0^{2\pi} \Delta x_2(\varphi') (\cos n\varphi' \sin n\varphi - \sin n\varphi' \cos n\varphi) d\varphi'$$

$$\Delta y_1(\varphi) = b_0 + \frac{1}{\pi} \sum_{n=1}^{\infty} \frac{q^n + q^{-n}}{q^n - q^{-n}} \int_0^{2\pi} \Delta x_1(\varphi') \sin n(\varphi' - \varphi) d\varphi'$$

$$- \frac{1}{\pi} \sum_{n=1}^{\infty} \frac{2}{q^n - q^{-n}} \int_0^{2\pi} \Delta x_2(\varphi') \sin n(\varphi' - \varphi) d\varphi' \quad (A6)$$

Now let $f(\varphi)$ be a function that can be developed in a Fourier series for $0 \leq \varphi \leq 2\pi$. Then

$$\int_0^{2\pi} f(\varphi') \frac{1}{2} \cot\left(\frac{\varphi' - \varphi}{2}\right) d\varphi' = \sum_{m=1}^{\infty} \int_0^{2\pi} f(\varphi') \sin m(\varphi' - \varphi) d\varphi' \equiv 0 \quad (A7)$$

Hence,

$$\Delta Y_1(\phi) = b_0 + \frac{1}{\pi} \sum_{n=1}^{\infty} \int_0^{2\pi} \left\{ \left[\frac{q^n + q^{-n}}{q^n - q^{-n}} \Delta x_1(\phi') \sin n(\phi' - \phi) \right] - \Delta x_1(\phi') \left[\frac{1}{2} \cot \frac{(\phi' - \phi)}{2} - \sin n(\phi' - \phi) \right] \right\} d\phi ,$$

$$- \frac{1}{\pi} \sum_{n=1}^{\infty} \frac{2}{q^n - q^{-n}} \int_0^{2\pi} \Delta x_2(\phi') \sin n(\phi' - \phi) d\phi ,$$

or

$$\begin{aligned} \Delta Y_1(\phi) &= b_0 - \frac{1}{\pi} \sum_{n=1}^{\infty} \int_0^{2\pi} \Delta x_1(\phi') \left[\frac{1}{2} \cot \frac{(\phi' - \phi)}{2} + \frac{2q^{2n}}{1-q^{2n}} \sin n(\phi' - \phi) \right] d\phi , \\ &+ \frac{1}{\pi} \sum_{n=1}^{\infty} \int_0^{2\pi} \frac{2q^n}{1-q^{2n}} \Delta x_2(\phi') \sin n(\phi' - \phi) d\phi , \end{aligned} \quad (\text{A8})$$

Inasmuch as the series of equation (A8) are uniformly convergent as are the series of equations (5), the summation and integration may be interchanged in equation (A8) to yield equation (5).

APPENDIX B

THE NUMERICAL EVALUATION OF THE CARTESIAN MAPPING FUNCTION

The determination of the functions Δx_1 and Δx_2 from the given functions Δy_1 and Δy_2 was based in this paper on numerical integration of the first two equations (5). The equations for Δx_1 and Δx_2 , when the constant a_0 has been set equal to zero, are

$$\left. \begin{aligned} \Delta x_1(\varphi) &= \frac{1}{\pi} \int_0^{2\pi} \Delta y_1(\varphi') \left[\frac{1}{2} \cot \frac{(\varphi' - \varphi)}{2} + \sum_{n=1}^{\infty} \frac{2q^{2n}}{1-q^{2n}} \sin n(\varphi' - \varphi) \right] d\varphi' \\ &\quad - \frac{1}{\pi} \int_0^{2\pi} \Delta y_2(\varphi') \sum_{n=1}^{\infty} \frac{2q^n}{1-q^{2n}} \sin n(\varphi' - \varphi) d\varphi' \\ \Delta x_2(\varphi) &= - \frac{1}{\pi} \int_0^{2\pi} \Delta y_2(\varphi') \left[\frac{1}{2} \cot \frac{(\varphi' - \varphi)}{2} + \sum_{n=1}^{\infty} \frac{2q^{2n}}{1-q^{2n}} \sin n(\varphi' - \varphi) \right] d\varphi' \\ &\quad + \frac{1}{\pi} \int_0^{2\pi} \Delta y_1(\varphi') \sum_{n=1}^{\infty} \frac{2q^n}{1-q^{2n}} \sin n(\varphi' - \varphi) d\varphi' \end{aligned} \right\} (B1)$$

If the range of φ is divided into $2n$ equal intervals whose length is δ , if the values of Δy are given at the end points of the intervals, and if Δx is desired at the same points, approximate integration will yield expressions of the following form:

$$\left. \begin{aligned} \Delta x_1(\varphi) &= \sum_{k=0}^{2n-1} (c_k + d_k) \Delta y_1(\varphi + k\delta) + \sum_{k=0}^{2n-1} e_k \Delta y_2(\varphi + k\delta) \\ \Delta x_2(\varphi) &= - \sum_{k=0}^{2n-1} (c_k + d_k) \Delta y_2(\varphi + k\delta) - \sum_{k=0}^{2n-1} e_k \Delta y_1(\varphi + k\delta) \end{aligned} \right\} (B2)$$

The values of c_k have been calculated in reference 1 by means of Simpson's rule and other simplifications for use with the CMF of simply connected regions. The values of d_k and e_k may be similarly obtained. The value of c_k as calculated in reference 1 is

$$c_0 = 0$$

$$c_1 = \frac{\delta}{6\pi} \cot \frac{\delta}{2} + \frac{\delta + \sin \delta}{2\pi \sin \delta}$$

$$c_{2n-1} = \frac{-\delta}{6\pi} \cot \frac{\delta}{2} - \frac{\delta + \sin \delta}{2\pi \sin \delta}$$

$$c_k = \frac{\delta}{3\pi} \cot \frac{k\delta}{2} \quad (k \text{ odd})$$

$$c_k = \frac{2\delta}{3\pi} \cot \frac{k\delta}{2} \quad (k \text{ even})$$

In the present paper, because the number of intervals was an integral multiple of 6, Weddle's rule was used for the evaluation of d_k and e_k .

The values of c_k are given in table 4 for the cases of $2n = 24$ and $2n = 48$. The values of d_k and e_k contain the parameter q . Hence, these coefficients must be evaluated anew for each approximation.

REFERENCES

1. Perl, W., and Moses, H. E.: Velocity Distributions on Symmetrical Airfoils in Closed Tunnels by Conformal Mapping. NACA ARR No. E6H23, 1946.
2. Mutterperl, William: The Conformal Transformation of an Airfoil into a Straight Line and Its Application to the Inverse Problem of Airfoil Theory. NACA ARR No. L4K22a, 1944.
3. Garrick, I. E.: Potential Flow about Arbitrary Biplane Wing Sections. NACA Rep. No. 542, 1936.

4. Goldstein, S.: Steady Two-Dimensional Flow past a Solid Cylinder in a Non-Uniform Stream and Two-Dimensional Wind-Tunnel Interference. R. & M. No. 1902, British A.R.C., 1942.
5. Tannery, Jules, and Molk, Jules: *Éléments de la Théorie des Fonctions Elliptiques*. Gauthier-Villars et Fils (Paris), 1893-1902.
6. Villat, Henri: Le Problème de Dirichlet dans une Aire Annulaire. *Rendiconti del Circolo Mat. di Palermo*, vol. 33, 1912, pp. 134-175.
7. Tomotika, Susumu: The Lift on a Flat Plate Placed in a Stream between Two Parallel Walls and Some Allied Problems. Tokyo Imperial Univ., Aero. Res. Inst. Rep. No. 101, vol. 8, no. 5, Jan. 1934, pp. 157-227.
8. Havelock, T. H.: The Lift and Moment on a Flat Plate in a Stream of Finite Width. *Proc. Roy. Soc. (London)*, ser. A., vol. 166, no. 925, May 18, 1938, pp. 178-196.
9. Glauert, H.: Wind Tunnel Interference on Wings, Bodies and Airscrews. R. & M. No. 1566, British A.R.C., 1933.
10. Klein, Milton M.: Methods of Obtaining Data in the Langley Two-Dimensional Low-Turbulence Tunnel. Appendix of NACA ACR No. L5C05 by Ira H. Abbott, Albert E. von Doenhoff, and Louis S. Stivers, Jr., 1945.

TABLE 1. - ORDINATES OF 12-PERCENT THICK AIRFOIL

[From table I of reference 1]

Station (percent chord from nose)	Ordinate	Station (percent chord from nose)	Ordinate
0	0	50	5.880
1.25	1.425	55	5.540
2.5	1.900	60	5.025
5	2.585	65	4.415
10	3.540	70	3.750
15	4.250	75	3.060
20	4.820	80	2.350
25	5.295	85	1.685
30	5.655	90	1.060
35	5.900	95	.510
40	6.000	97.5	.260
45	6.010	100	0

National Advisory Committee
for Aeronautics

TABLE 2.- VELOCITY DISTRIBUTION AND CARTESIAN MAPPING FUNCTION FOR AIRFOIL AT ANGLE OF ATTACK OF 0°

$$[q = 0.2041; \varphi_N = 90^\circ; \varphi_T = 270^\circ; \varphi_2 = 90^\circ; \tau = -0.0067]$$

φ (deg)	Airfoil				Channel walls							
	$4x_1$	$\frac{v_{\varphi 1}}{V}$	Δy_1	Δx_1	$\frac{d\Delta x_1}{d\varphi}$	$\frac{d\Delta y_1}{d\varphi}$	$4x_2$	$\frac{v_{\varphi 2}}{V}$	Δy_2	Δx_2	$\frac{d\Delta x_2}{d\varphi}$	$\frac{d\Delta y_2}{d\varphi}$
0 x 15	-0.0456	1.1764	-0.02978	-0.00470	0.0392	-0.0069	-0.0286	1.0312	0	-0.00045	0.0113	0
1	-2751	1.1657	-0.02955	-0.00555	0.0363	.0076	-0.4112	1.0299	0	.00251	.0111	0
2	-4968	1.1511	-0.02640	-0.01449	0.0315	.0166	-0.8152	1.0256	0	.00536	.0104	0
3	-6976	1.1200	-0.02115	-0.02148	0.0227	.0220	-1.2740	1.0179	0	.00786	.0086	0
4	-8601	1.1085	-0.01495	-0.02650	0.0168	.0256	-1.8559	1.0094	0	.00980	.0062	0
5	-9647	1.0121	-0.00818	-0.02999	.0097	.0283	-2.7777	1.0027	0	.01104	.0033	0
6	-1.0002	0	0	-0.03142	0	.0295	-0.0000	1.0000	0	.01146	0	0
7	-9647	1.0121	-0.00818	-0.02999	-0.0097	.0283	-2.7777	1.0027	0	.01104	-0.0033	0
8	-8601	1.1085	-0.01495	-0.02650	-0.0168	.0256	-1.8559	1.0094	0	.00980	-0.0062	0
9	-6976	1.1200	-0.02115	-0.02148	-0.0227	.0220	-1.2740	1.0179	0	.00786	-0.0086	0
10	-4968	1.1511	-0.02640	-0.01449	-0.0315	.0166	-0.8152	1.0256	0	.00536	-0.0104	0
11	-2751	1.1657	-0.02955	-0.00555	-0.0363	.0076	-0.4112	1.0299	0	.00251	-0.0111	0
12	-456	1.1764	-0.02978	-0.00470	-0.0392	-0.069	-0.0286	1.0312	0	-0.0045	-0.0113	0
13	-1854	1.1383	-0.02558	-0.01457	-0.0325	-0.0266	-0.3544	1.0280	0	-0.00330	-0.0104	0
14	-4184	1.0559	-0.01803	-0.02067	-0.0143	-0.0290	-0.7599	1.0214	0	-0.00583	-0.0087	0
15	-6395	0.9994	-0.01028	-0.02261	-0.0017	-0.0269	1.2204	1.0142	0	-0.00787	-0.0069	0
16	-8249	0.9471	-0.00435	-0.02190	-0.0073	-0.0168	1.8043	1.0071	0	-0.00935	-0.0047	0
17	-9515	.8817	-0.00103	-0.01989	.0101	-0.0080	2.7277	1.0020	0	-0.01025	-0.0025	0
18	1.0001	0	0	-0.01803	0	0	-0.0000	1.0000	0	-0.01054	0	0
19	9515	0.8817	-0.00103	-0.01989	-0.0101	-0.0080	2.7277	1.0020	0	-0.01025	0.0025	0
20	8249	0.9471	-0.00435	-0.02190	-0.0073	-0.0168	1.8043	1.0071	0	-0.00935	.0047	0
21	6395	0.9994	-0.01028	-0.02261	-0.0017	-0.0269	1.2204	1.0142	0	-0.00787	.0069	0
22	-4184	1.0559	-0.01803	-0.02067	.0143	-0.0290	0.7599	1.0214	0	-0.00582	.0087	0
23	-1854	1.1383	-0.02558	-0.01457	.0325	-0.0266	0.3544	1.0280	0	-0.00330	.0104	0

TABLE 3.- VELOCITY DISTRIBUTION AND CARTESIAN MAPPING
FUNCTION FOR AIRFOIL AT ANGLE OF ATTACK OF 4°

[$q = 0.2041$; $\phi_N = 94^\circ$; $\phi_T = 274^\circ$; $\phi_2 = 89.91^\circ$; $\tau = -0.0063$]

ϕ (deg)	Airfoil						Channel walls					
	$4x_1$	$\frac{v_{c1}}{V}$	$r(\phi)$	Δx_1	$\frac{d\Delta x_1}{d\phi}$	$\frac{d\Delta y_1}{d\phi}$	$4x_2$	$\frac{v_{c2}}{V}$	Δy_2	Δx_2	$\frac{d\Delta x_2}{d\phi}$	$\frac{d\Delta y_2}{d\phi}$
0 x 7.5	0.0152	1.0735	-0.02940	0.01005	0.0376	0.0033	0.0236	0.9730	0	0.00591	0.0114	0
1	-.1010	1.0709	-.02840	.01511	.0372	.0110	-.1917	.9719	0	.00739	.0109	0
2	-.2168	1.0617	-.02615	.01983	.0355	.0165	-.3850	.9703	0	.00875	.0101	0
3	-.3308	1.0419	-.02380	.02115	.0316	.0244	-.5838	.9686	0	.01000	.0090	0
4	-.4417	1.0133	-.02028	.02795	.0260	.0291	-.7920	.9670	0	.01107	.0070	0
5	-.5486	.9822	-.01622	.03095	.0203	.0330	-.1.0134	.9659	0	.01198	.0062	0
6	-.6493	.9464	-.01182	.03317	.0145	.0356	-.1.2549	.9657	0	.01267	.0045	0
7	-.7415	.9036	-.00720	.03465	.0088	.0369	-.1.5261	.9668	0	.01316	.0027	0
8	-.8234	.8247	-.00212	.03528	-.0013	.0355	-.1.8436	.9697	0	.01340	.0010	0
9	-.8928	.7729	-.00212	.03502	-.0020	.0313	-.2.2367	.9743	0	.01342	-.0009	0
10	-.9448	.6579	.00598	.03464	-.0030	.0303	-.2.7752	.9810	0	.01319	-.0027	0
11	-.9776	.3130	.01035	.03418	-.0082	.0347	-.3.6780	.9896	0	.01272	-.0045	0
12	-.9950	.5485	.01525	.03241	-.0194	.0338	-.9.2779	1.0001	0	.01202	-.0062	0
13	-.9963	1.7756	.01925	.02917	-.0229	.0299	-.3.6554	1.0121	0	.01109	-.0079	0
14	-.9777	1.6934	.02312	.02634	-.0252	.0250	-.2.7736	1.0249	0	.00997	-.0094	0
15	-.9407	1.5167	.02600	.02294	-.0275	.0210	-.2.2162	1.0379	0	.00864	-.0106	0
16	-.8875	1.4150	.02862	.01915	-.0295	.0183	-.1.8613	1.0506	0	.00718	-.0118	0
17	-.8188	1.3589	.03075	.01518	-.0315	.0155	-.1.5513	1.0624	0	.00555	-.0127	0
18	-.7375	1.3249	.03252	.01096	-.0333	.0121	-.1.2863	1.0731	0	.00384	-.0135	0
19	-.6456	1.3042	.03390	.00652	-.0350	.0085	-.1.0503	1.0817	0	.00203	-.0140	0
20	-.5455	1.2910	.03475	.00184	-.0365	.0048	-.8.330	1.0883	0	.00021	-.0142	0
21	-.4391	1.2843	.03522	-.00305	-.0380	.0005	-.6.288	1.0926	0	-.00164	-.0141	0
22	-.3287	1.2803	.03502	-.00824	-.0392	-.0047	-.4.326	1.0948	0	-.00343	-.0138	0
23	-.2152	1.2790	.03402	-.01349	-.0102	-.0101	-.2.414	1.0944	0	-.00518	-.0131	0
24	-.1004	1.2772	.03235	-.01883	-.0106	-.0162	-.0.272	1.0918	0	-.00680	-.0120	0
25	.0143	1.2652	.02970	-.02123	-.0390	-.0250	-.1.375	1.0874	0	-.00831	-.0107	0
26	.1287	1.2392	.02558	-.02926	-.0350	-.0364	-.3.303	1.0814	0	-.00963	-.0092	0
27	.2439	1.1935	.02038	-.03325	-.0263	-.0128	-.5.290	1.0745	0	-.01079	-.0077	0
28	.3592	1.1455	.01438	-.03590	-.0160	-.0156	-.7.370	1.0667	0	-.01171	-.0061	0
29	.4732	1.0927	.00828	-.03712	-.0041	-.0162	-.9.585	1.0576	0	-.01243	-.0042	0
30	.5834	1.0475	.00215	-.03695	-.0065	-.0141	1.2000	1.0491	0	-.01290	-.0027	0
31	.6871	1.0093	-.00325	-.03558	-.0153	-.0395	1.4711	1.0400	0	-.01314	-.0010	0
32	.7812	.9805	-.00815	-.03317	-.0216	-.0314	1.7876	1.0308	0	-.01315	.0008	0
33	.8621	.9564	-.01178	-.03007	-.0253	-.0240	2.1793	1.0221	0	-.01294	.0023	0
34	.9260	.9328	-.01450	-.02674	-.0269	-.0175	2.7132	1.0139	0	-.01252	.0039	0
35	.9708	.9223	-.01612	-.02332	-.0254	-.0110	3.6019	1.0066	0	-.01190	.0053	0
36	.9948	.9246	-.01712	-.01996	-.0225	-.0043	9.2833	1.0001	0	-.01112	.0066	0
37	.9953	.8741	-.01750	-.01723	-.0185	0	3.6385	.9946	0	-.01016	.0078	0
38	.9723	.8882	-.01760	-.01526	-.0140	-.0012	2.7416	.9900	0	-.00907	.0088	0
39	.9280	.9050	-.01792	-.01370	-.0115	-.0030	2.2091	.9864	0	-.00785	.0096	0
40	.8653	.9190	-.01850	-.01229	-.0102	-.0051	1.8208	.9836	0	-.00654	.0104	0
41	.7861	.9307	-.01932	-.01099	-.0099	-.0080	1.5084	.9814	0	-.00511	.0110	0
42	.6932	.9427	-.02050	-.00968	-.0107	-.0116	1.2411	.9800	0	-.00362	.0116	0
43	.5898	.9608	-.02218	-.00813	-.0136	-.0141	1.0030	.9789	0	-.00206	.0120	0
44	.4796	.9876	-.02425	-.00594	-.0190	-.0148	.7842	.9780	0	-.00048	.0123	0
45	.3653	1.0142	-.02620	-.00300	-.0248	-.0146	.5784	.9772	0	-.00116	.0124	0
46	.2485	1.0414	-.02786	-.00061	-.0308	-.0127	.3809	.9762	0	-.00276	.0123	0
47	.1314	1.0669	-.02920	-.00501	-.0362	-.0064	.1887	.9748	0	-.00437	.0120	0

TABLE 4. - COEFFICIENTS FOR CALCULATION OF CARTESIAN
MAPPING FUNCTION FOR SINGLE CONTOUR

(a) 24-point scheme

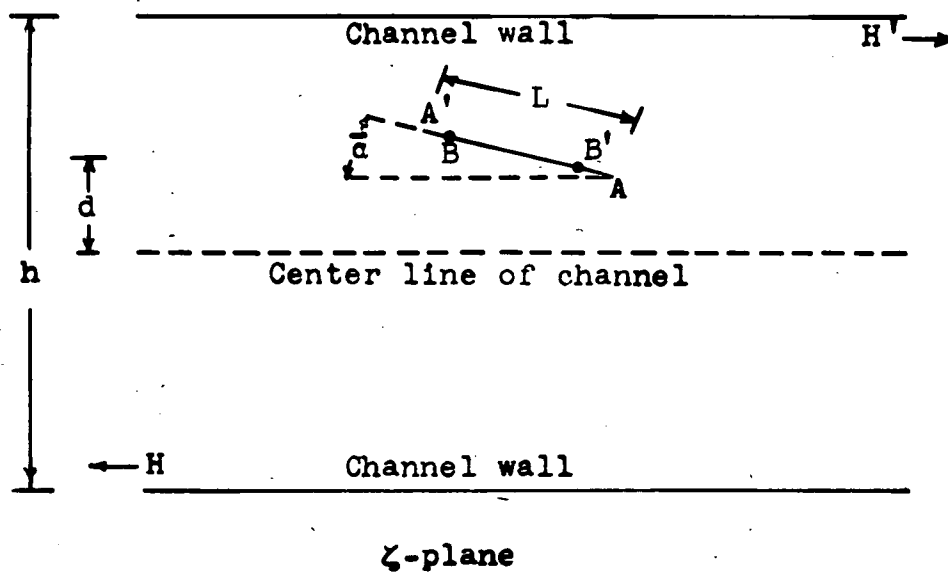
k	c_k	k	c_k
0	0	12	0
1	.42564	13	-.00366
2	.20734	14	-.01489
3	.06706	15	-.01151
4	.09623	16	-.03208
5	.03620	17	-.02131
6	.05556	18	-.05556
7	.02131	19	-.03620
8	.03203	20	-.09623
9	.01151	21	-.06706
10	.01489	22	-.20734
11	.00366	23	-.42564

(b) 48-point scheme

k	c_k	k	c_k
0	0	24	0
1	.42470	25	-.00091
2	.21099	26	-.00366
3	.06982	27	-.00276
4	.10367	28	-.00744
5	.04092	29	-.00472
6	.06706	30	-.01151
7	.02616	31	-.00685
8	.04811	32	-.01604
9	.02079	33	-.00928
10	.03620	34	-.02132
11	.01584	35	-.01218
12	.02778	36	-.02778
13	.01218	37	-.01584
14	.02132	38	-.03620
15	.00928	39	-.02079
16	.01604	40	-.04811
17	.00685	41	-.02816
18	.01151	42	-.06706
19	.00472	43	-.04092
20	.00744	44	-.10367
21	.00276	45	-.06982
22	.00366	46	-.21099
23	.00091	47	-.42470

NACA RM NO. E7A28

Fig. 1



NATIONAL ADVISORY
COMMITTEE FOR AERONAUTICS

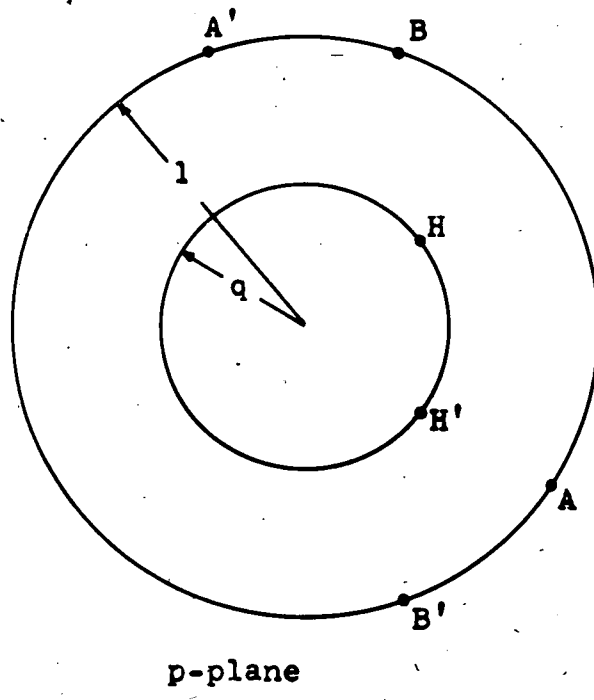


Figure 1.- Transformation of flat plate and channel into two concentric circles.

Fig. 2

NACA RM NO. E7A28

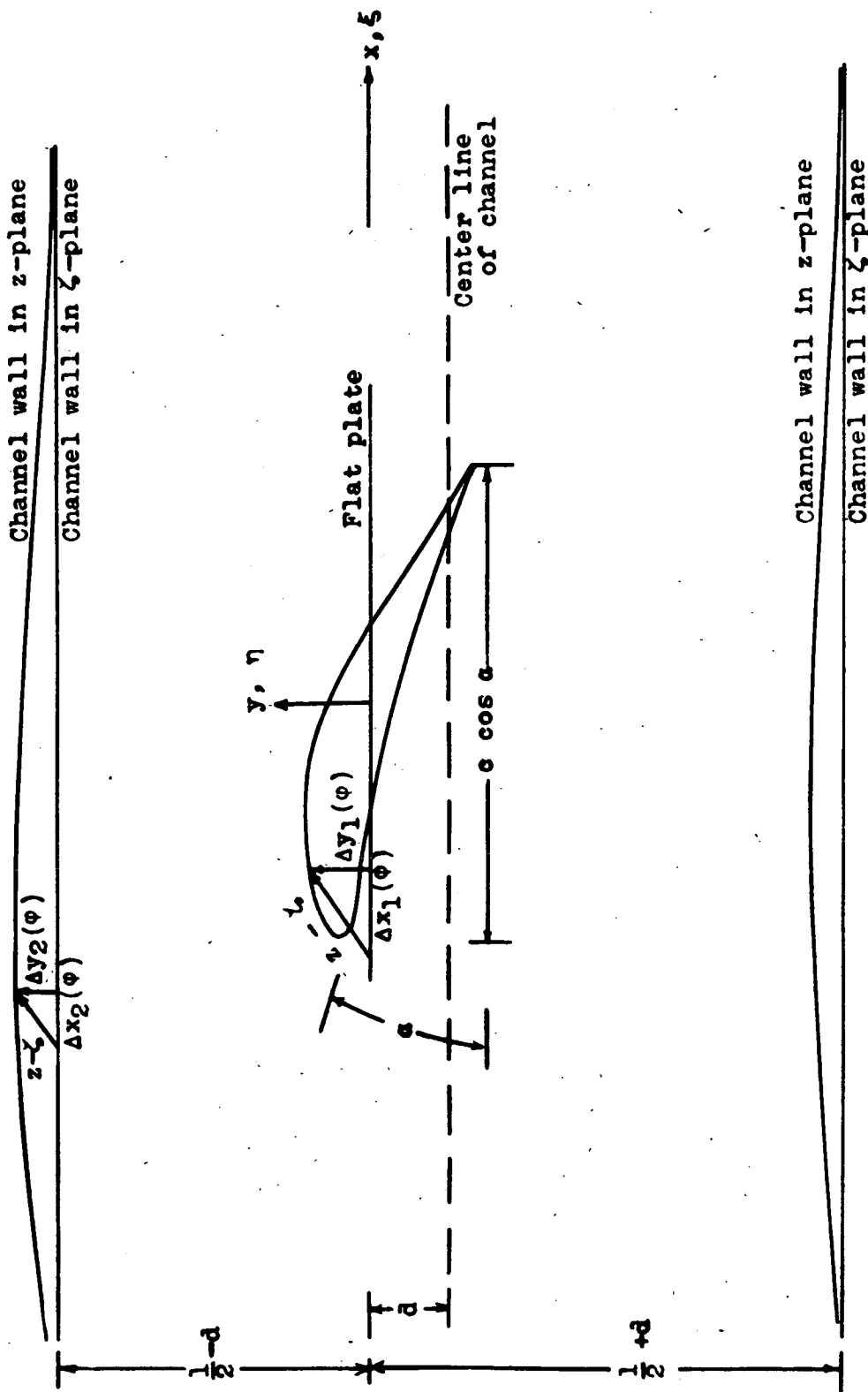


Figure 2.— Transformation of airfoil and arbitrary channel into flat plate and plane-walled channel by Cartesian mapping function.

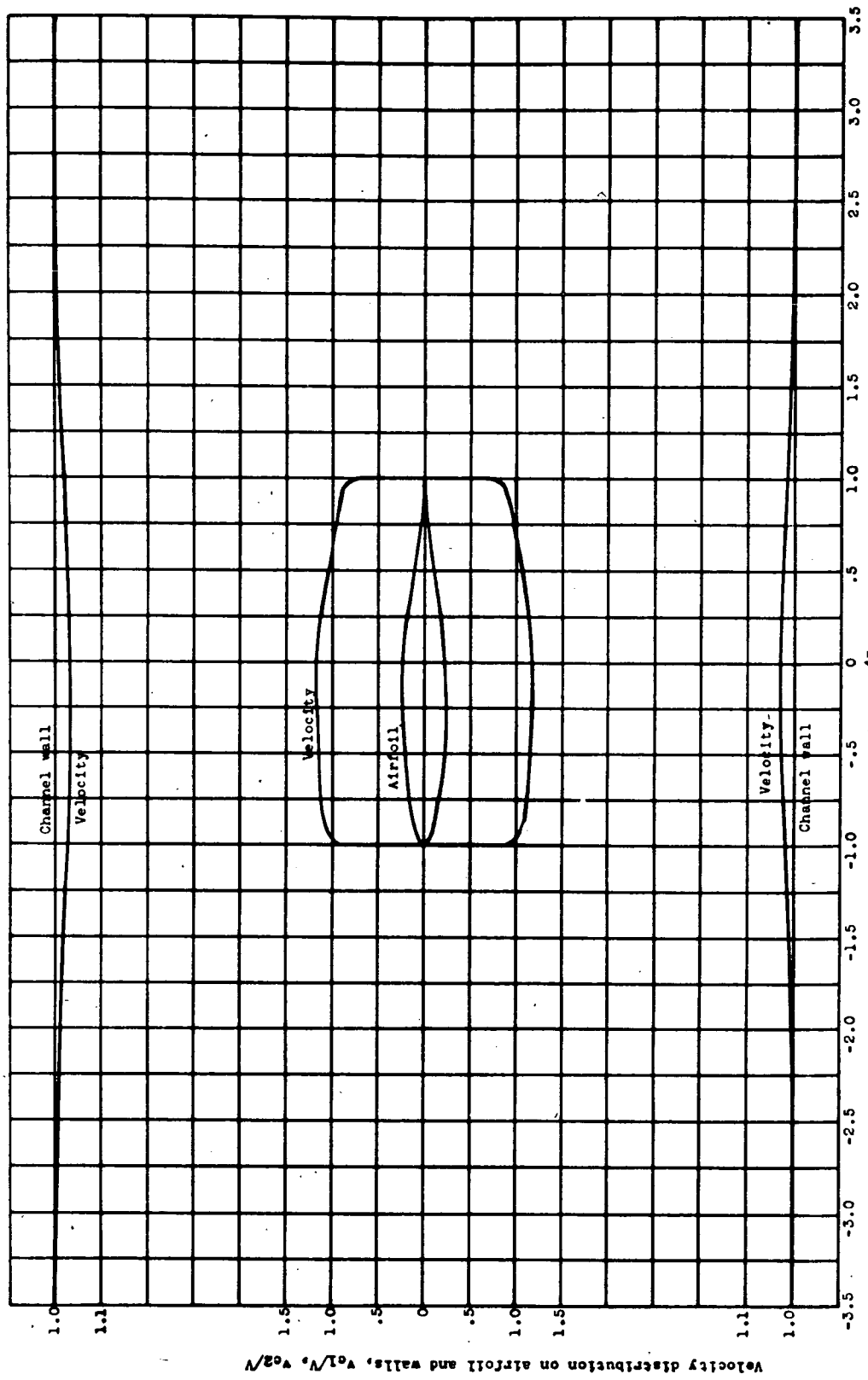


FIGURE 3.— Velocity distribution on airfoil in channel at angle of attack of 0° and velocity distribution on channel walls.

Fig. 4

NACA RM NO. E7 A28

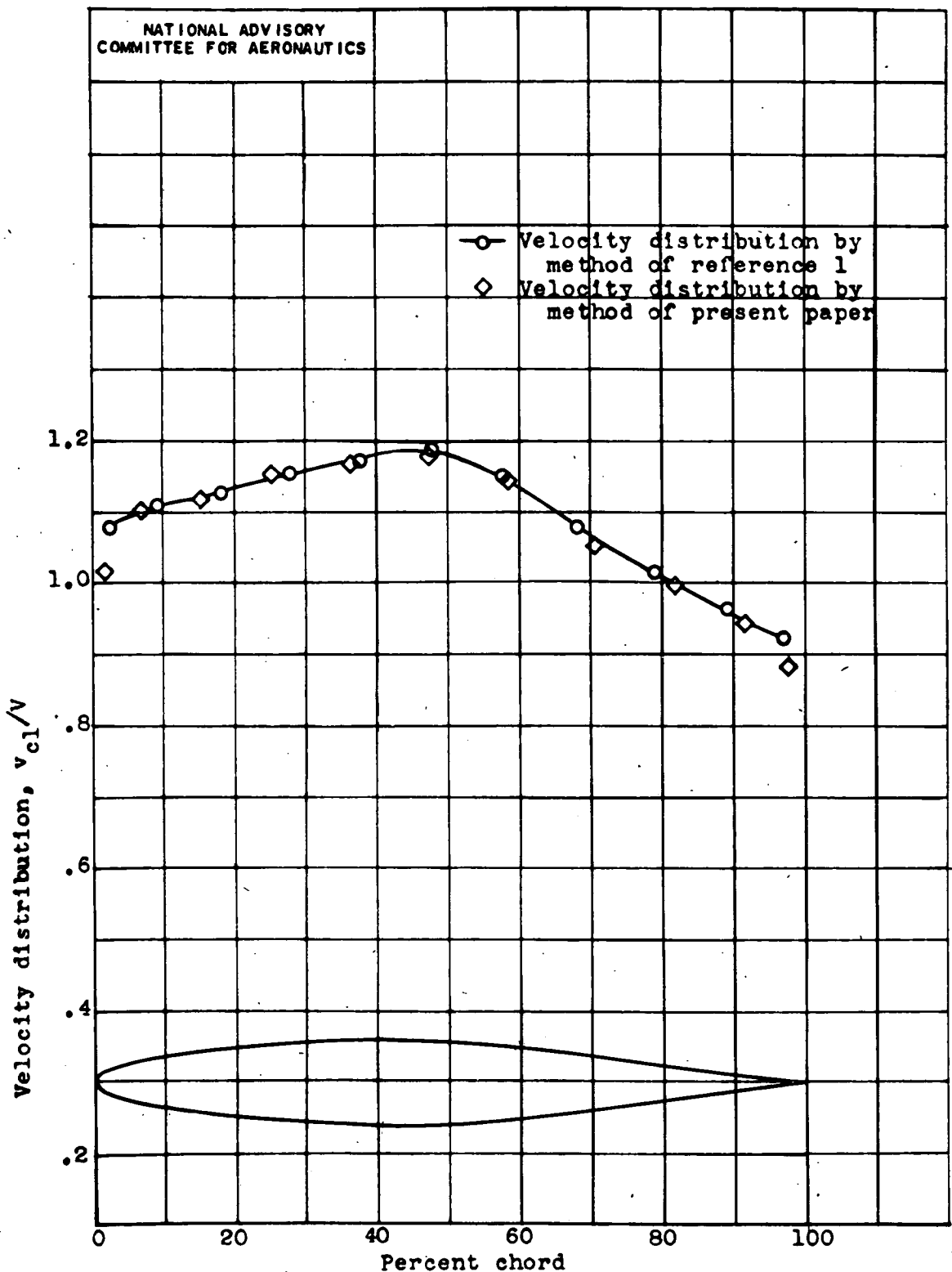


Figure 4.— Comparison of velocity distributions in channel obtained by two methods.

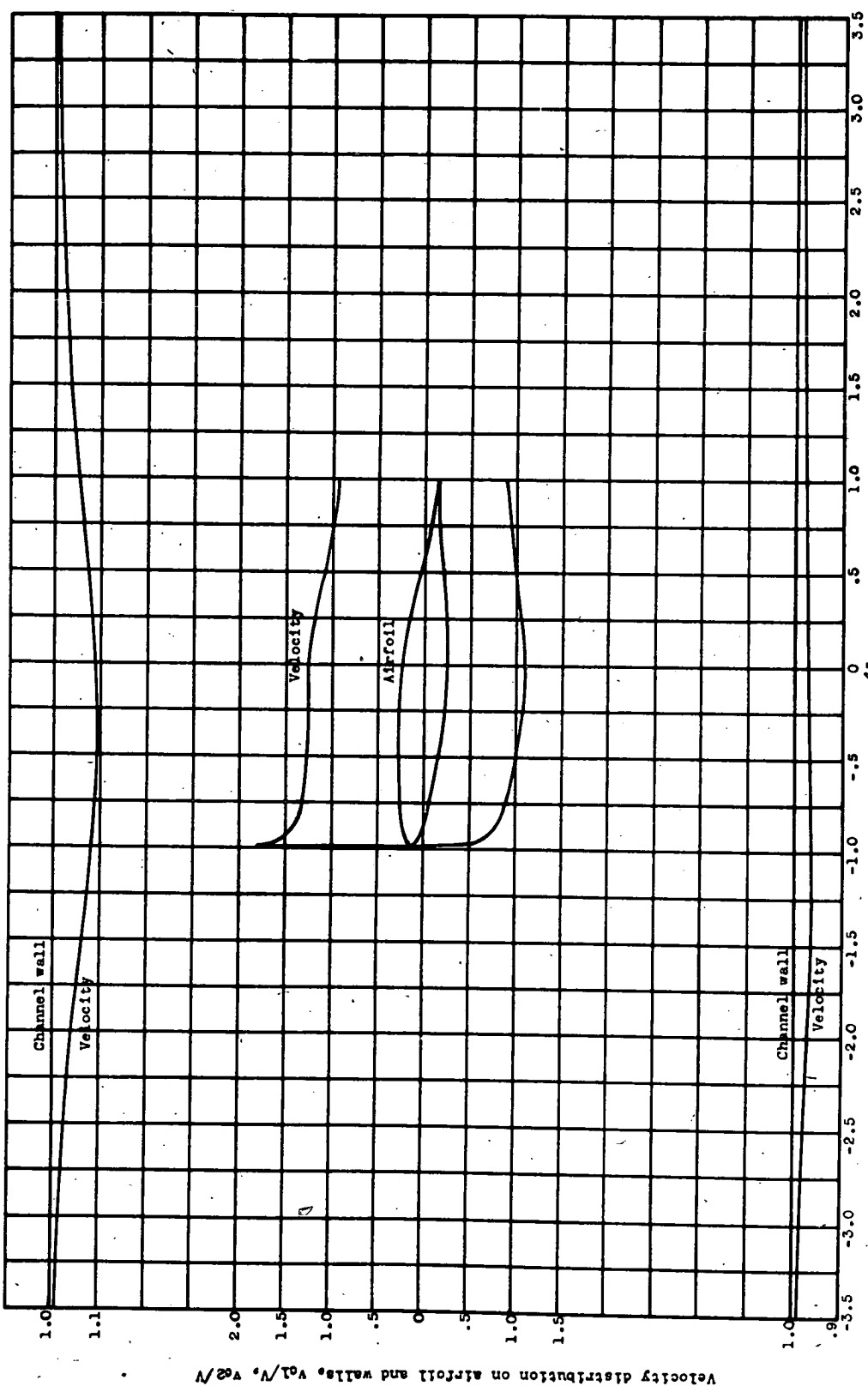


Figure 5. Velocity distribution on airfoil in channel at angle of attack of 4° and velocity distribution on channel walls.

Fig. 6

NACA RM NO. E7A28

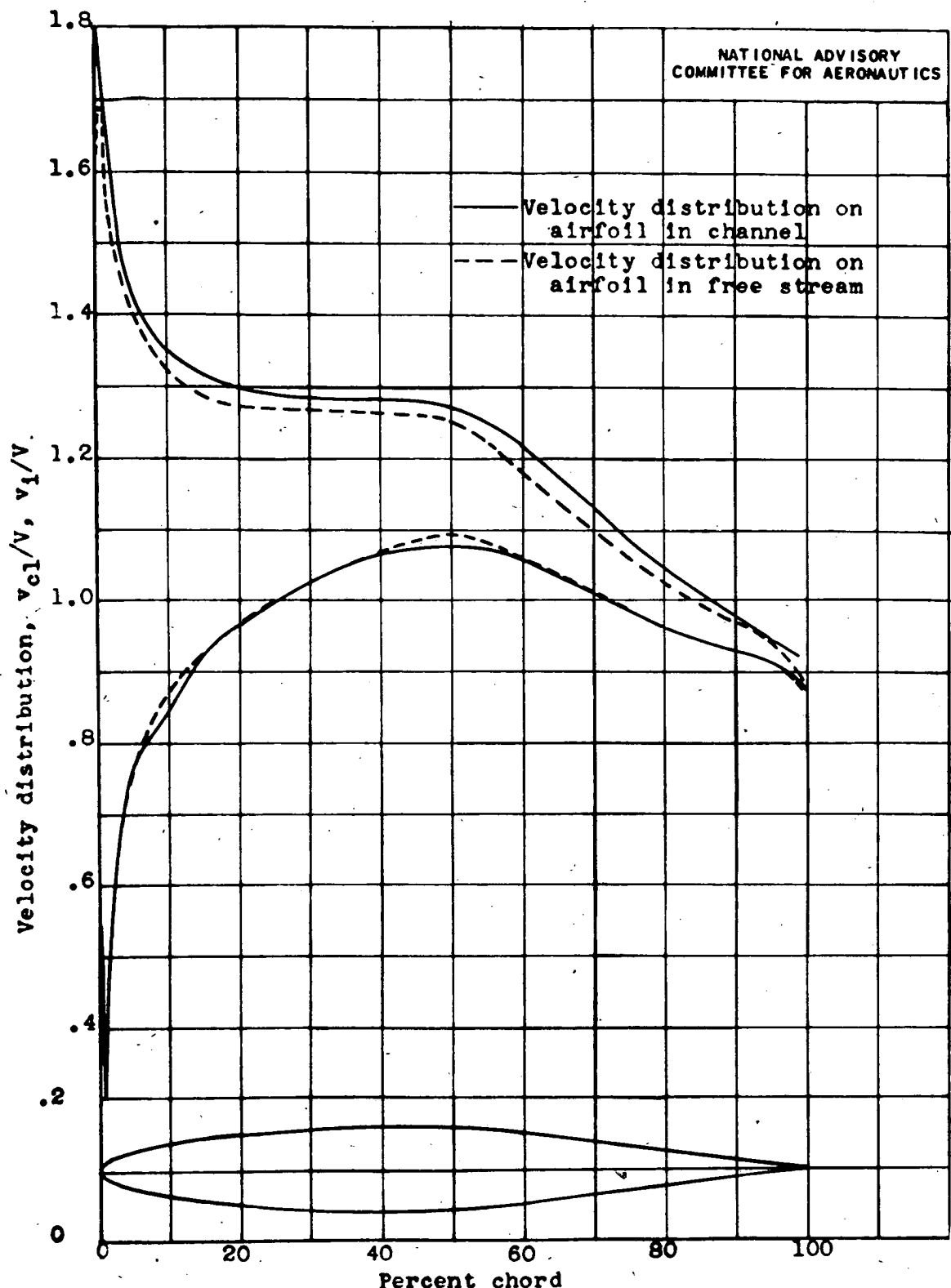
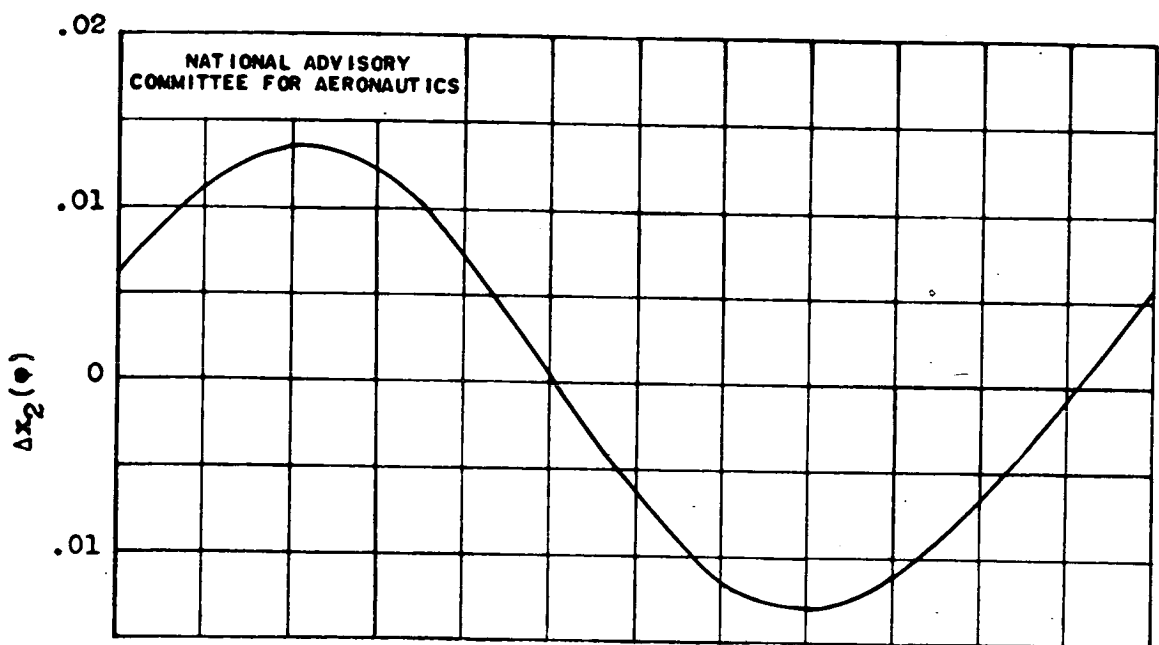
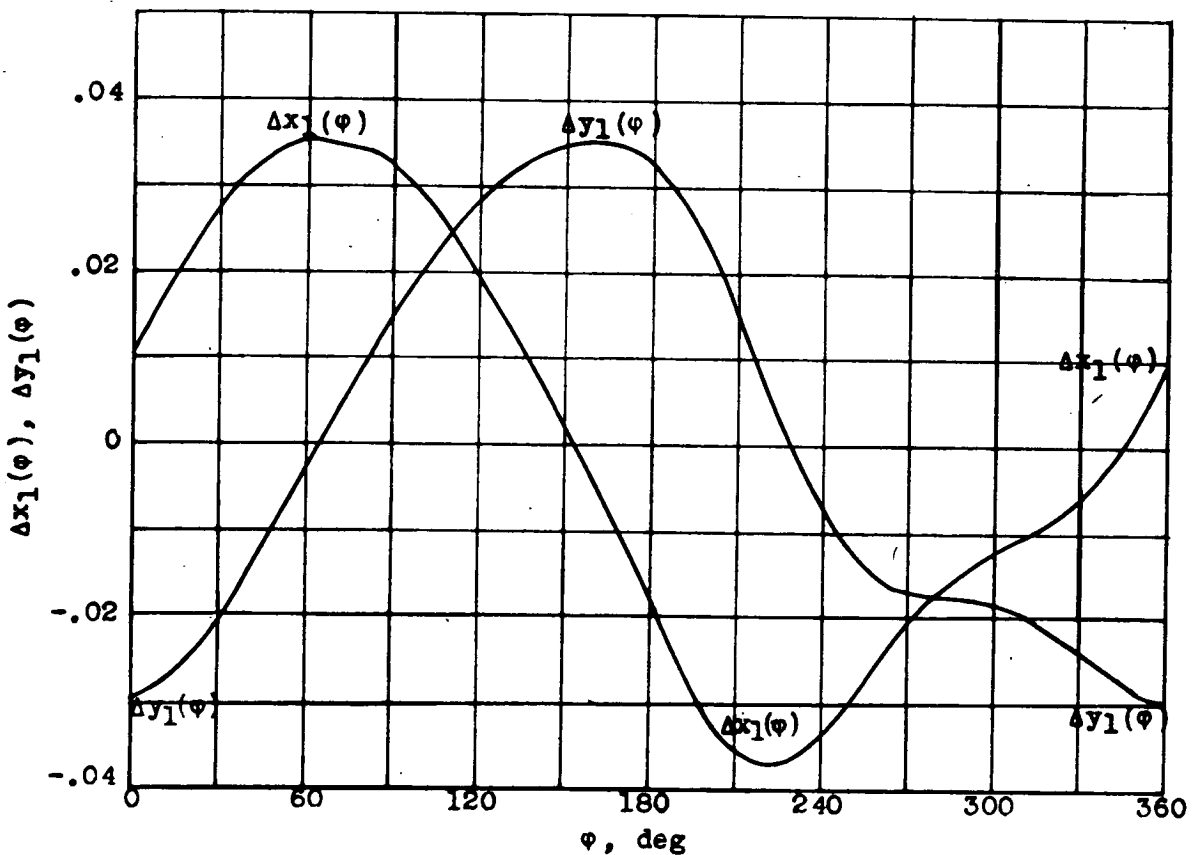


Figure 6.- Comparison of velocities on airfoil in free stream and on airfoil in channel for $\alpha = 4^\circ$.



(a) CMF on inner circle.

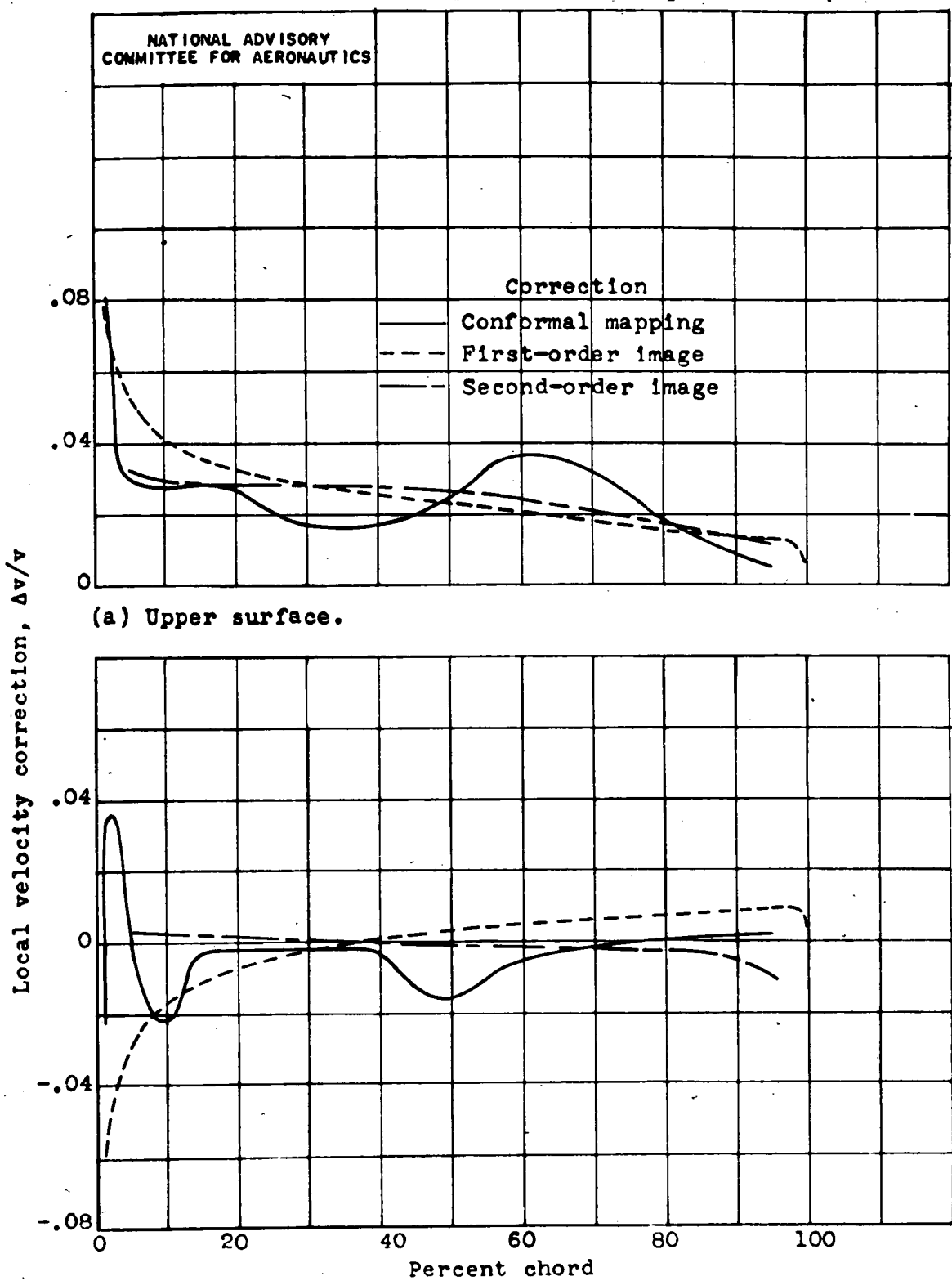


(b) CMF on outer circle.

Figure 7.- Cartesian mapping function for airfoil in a channel at $\alpha = 40^\circ$.

Fig. 8

NACA RM NO. E7 A28



(b) Lower surface.

Figure 8.— Velocity corrections for 12-percent-thick airfoil.
 $\alpha = 4^\circ$, $c/h = 0.5$.

NACA RM NO. E7A28

Fig. 9

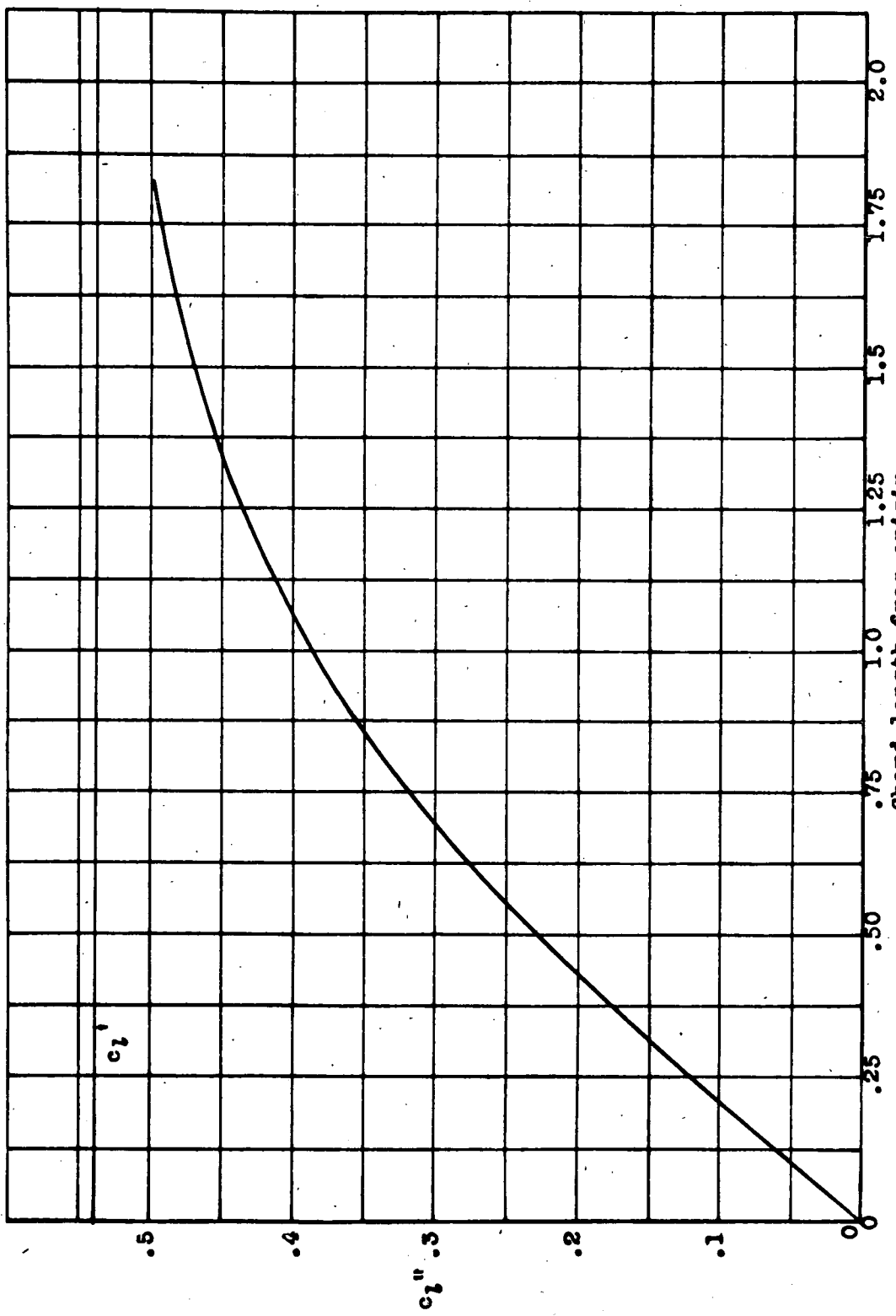


Figure 9.— Lift coefficient obtained from pressure distribution on walls as a function of limits of integration.

